The University of Sydney

School of Civil Engineering
Sydney NSW 2006
AUSTRALIA

http://www.civil.usyd.edu.au/

Centre for Advanced Structural Engineering

Shear Locking in Isoparametric Spline Finite Strips

Research Report No R876

Gabriele Eccher MEng
Kim J. R. Rasmussen MScEng PhD
Riccardo Zandonini MEng PhD

February 2007

The University of Sydney

School of Civil Engineering
Centre for Advanced Structural Engineering
http://www.civil.usyd.edu.au/

Shear Locking in Isoparametric Spline Finite Strips

Research Report No R876

Gabriele Eccher MEng
Kim J. R. Rasmussen MScEng PhD
Riccardo Zandonini MEng PhD

February 2007

Abstract:
The Mindlin plate bending theory includes shear deformations in the formulation to better reproduce the behaviour of thick plates and to avoid difficulties in satisfying continuity requirements along strip boundaries. Unfortunately, in many thin plate applications over-stiff solutions are encountered due to the development of spurious stiffness contributions in the numerical solution. This phenomenon is usually referred to as “locking” and if associated with an insufficient representation of bending and shear deformations is called “shear locking”. A method for testing the performance of finite elements with regard to shear locking is described. The method is called “the monomial test” and has been introduced by Briassoulis (1988) who applied it to a series of beam and plate elements. The monomial test is applied for the first time to the isoparametric spline finite strip method. The effect of shear locking on the performance of the isoparametric spline finite strip is investigated in detail as is the ameliorating influence of selective reduced integration. The influence of the order and magnitude of the distortion of the strip, the integration scheme and the number of longitudinal sections of the isoparametric spline finite strip are analysed. Numerical examples are included to illustrate the concepts described.

Keywords:
Shear locking, isoparametric spline finite strip method, thin plates, Mindlin theory, reduced integration, bending, shear.

Copyright Notice

School of Civil Engineering, Research Report R876
Shear Locking in Isoparametric Spline Finite Strips

G.Eccher@civil.usyd.edu.au, K.Rasmussen@civil.usyd.edu.au and Riccardo.Zandonini@ing.unitn.it

Published by:
School of Civil Engineering
The University of Sydney
Sydney NSW 2006
AUSTRALIA

February 2007

This report and other Research Reports published by The School of Civil Engineering are available on the Internet:

http://www.civil.usyd.edu.au

TABLE OF CONTENTS

Introduction

Beam elements based on Timoshenko theory and plate elements based on to Mindlin theory include shear deformation in their formulation. This inclusion not only aims at taking proper account of shear in thick element applications but also at avoiding difficulties in satisfying continuity requirements along element boundaries when rotations are calculated from the out-of-plane displacement as in Euler-Bernoulli beam or Kirchhoff plate theories. In formulations taking shear into account, the out-of-plane displacement and mid-surface rotations are considered as independent variables. Continuity in displacements and rotations along element interfaces can hence be achieved as in common C^0 elements.

Unfortunately, if shear deformable elements are applied to a range of thin beams or plates, over-stiff solutions have been encountered which diverge from classical solutions obtained from thin beam or thin plate theory. This over-stiff behaviour is usually termed “locking”. In particular, locking associated with an insufficient representation of bending and shear deformations is called “shear locking”. In these cases the locking phenomenon is strictly related to the development of spurious shear-strains which have no physical counterpart.
A general remedy to alleviate shear locking is to apply a reduced numerical integration. However, reduced integration may lead to the development of spurious kinematics modes, also called zero energy modes. An improved version of reduced integration is the so-called selective reduced integration which applies a reduced numerical integration scheme only to the shear terms. In many plate and beam elements it avoids locking without the development of spurious kinematics modes.

The present report aims to investigate the nature of shear locking and how selective reduced integration may be applied to overcome locking regardless of the thickness of the element. A method to test the tendency of a finite element to locking, the so called monomial test (Briassoulis, 1988), is presented and consequently applied to the isoparametric spline finite strip method. The performance of the isoparametric spline finite strip is investigated in detail. An analytical expression of the spurious shear strains is given for the case of strips with a single longitudinal section, as well as strips with multiple sections. Different interpolation schemes are presented and analysed. Furthermore, the performance of the isoparametric spline finite strip with regard to shear locking is tested using numerical examples. The importance of the integration scheme, the longitudinal discretization (number of sections, m), and the degree and magnitude of strip distortions are shown. As a result, guidelines for defining an optimal finite strip mesh are provided.

Spurious shear strain

The effect of shear locking is to produce over-stiff behaviour of the element in thin applications. In the limit of a very thin element, this trend leads to solutions where both the displacement and rotational degrees of freedom tend to zero.

The stiffening effect in the case of typical shear locking is entirely due to the development of spurious shear strains. This phenomenon is present also in thick element applications but it drastically increases in thin applications. The spurious strain energy contribution increases with decreasing thickness to the extent of dominating the total strain energy of the finite element system in very thin applications.

By splitting a general displacement field into a contribution free from shear strain, i.e. a so-called Kirchhoff field, $\mathbf{u}_b$, and a shear displacement field, $\mathbf{u}_s$, a measure of the shear locking effect in the finite element formulation can be expressed by means of a factor, C_{sl}, which is a function of the ratio between the shear strain energy and the bending strain energy produced by a Kirchhoff field, $\mathbf{u}_b$. The shear locking factor, C_{sl}, is defined according to Briassoulis (1989) as

$$C_{sl} = \left(1 + \frac{\mathbf{u}_b{}^T \mathbf{K}_s \mathbf{u}_b}{\mathbf{u}_b{}^T \mathbf{K}_b \mathbf{u}_b} \right)^{-1} \tag{1}$$

where $\mathbf{K}_s$ is the shear contribution and $\mathbf{K}_b$ the bending contribution to the finite element stiffness matrix $\mathbf{K}$. The shear strain energy developed under a non-zero pure Kirchhoff field is always spurious and strictly related to the development of spurious shear strain. Hence, (1) is an indicator of the energy-related error introduced by spurious shear strains in the finite element formulation. If no spurious shear strain develops, or if it vanishes at the integration points, the shear locking factor, C_{sl}, is identically one. Conversely, spurious shear strains lead to a decreasing value of the shear locking factor which vanishes when complete locking occurs, i.e. when the shear strain contribution to the strain energy of the finite element assembly becomes so large that the flexural strain energy can be considered as zero in comparison with machine precision.

In order to investigate how the slenderness of the element influences the shear locking phenomenon in a plate element, we may rewrite (1) as

$$C_{sl} = \left(1 + \frac{G}{E} \left(\frac{L}{t} \right)^2 f\left(\gamma_{xz}^b, \gamma_{yz}^b \right) \right)^{-1} \tag{2}$$

In (2) the dependency of the shear locking coefficient to the aspect ratio of the element is isolated. The contribution G/Et^2 is due to the ratio between the shear and the flexural stiffness of a plate element, L^2 is proportional to the element mid-plane area while in the final term $f\left(\gamma_{xz}^b, \gamma_{yz}^b\right)$, the contributions related to spurious shear strains are collected. Again, no shear locking develops

only if no spurious shear strains develop, i.e. if $f\left(\gamma_{xz}^{b},\gamma_{yz}^{b}\right)=0$, but we may note here how, once spurious shear strain develops, the shear locking, expressed by means of the shear locking factor, C_{sl}, is a continuous function of the slenderness ratio *L*/*t* squared. For low values of the slenderness ratio, i.e. for thick element applications, spurious shear strains only lead to moderate stiffening effects. However, they increase rapidly in thin element applications until the machine precision is reached and full locking of the element is experienced.

A more precise definition of the spurious shear strain is here offered dealing with both thin and thick element applications. For simplicity the calculations are carried out only for the *yz* component of the shear strain. The extension to the *xz* component is straightforward.

The behaviour of a general C^0 plate element under a general displacement field may be decomposed into a contribution from the pure bending of the element and one related to the effect of shear strain. It is then possible to study the flexural behaviour separately from the shearing behaviour of the element (Briassoulis, 1989). For this purpose, the general displacement field is decomposed into a Kirchhoff field representing the flexural behaviour, identified by the superscript "*b*", and a field produced by the shear strain, identified by the superscript "*s*". The different fields are defined as

$$w = w^b + w^s \tag{3}$$

$$\theta = \theta^b \tag{4}$$

We note how the rotational field is entirely defined by the flexural Kirchhoff contribution for which the relation

$$\theta^b = \frac{\partial w^b}{\partial y} \tag{5}$$

holds everywhere. This implies that the contribution to the shear strain coming from the Kirchhoff part of the field is identically zero. Expressing (5) in natural coordinates (*a* and *b* in plate elements) we get

$$\theta^b = J_{21}^{-1}\frac{\partial w^b}{\partial a} + J_{22}^{-1}\frac{\partial w^b}{\partial b} \tag{6}$$

where J_{ij}^{-1} are the components of the inverse Jacobean matrix.

According to the finite element method, displacements and rotations, respectively, are expressed by

$$w = \sum_{i=1}^{n} N_i w_i = \sum_{i=1}^{n} N_i w_i^b + \sum_{i=1}^{n} N_i w_i^s \tag{7}$$

$$\theta = \sum_{i=1}^{n} N_i \theta_i = \sum_{i=1}^{n} N_i \theta_i^b \tag{8}$$

where *n* represents the number of nodes of the element.
The shear strain in the *y*-*z* plane is defined as

$$\begin{aligned} \gamma_{yz} &= \frac{\partial w}{\partial y} - \theta \\ &= J_{21}^{-1}\left(\sum_{i=1}^{n} \frac{\partial N_i}{\partial a} w_i \right) + J_{22}^{-1}\left(\sum_{i=1}^{n} \frac{\partial N_i}{\partial b} w_i \right) - \sum_{i=1}^{n} N_i \theta_i \end{aligned} \tag{9}$$

Introducing now the split displacement field described in (3) and (4) we get

$$\begin{aligned} \gamma_{yz} = {} & J_{21}^{-1}\left(\sum_{i=1}^{n} \frac{\partial N_i}{\partial a} w_i^b \right) + J_{22}^{-1}\left(\sum_{i=1}^{n} \frac{\partial N_i}{\partial b} w_i^b \right) - \sum_{i=1}^{n} N_i \theta_i^b + \\ & + J_{21}^{-1}\left(\sum_{i=1}^{n} \frac{\partial N_i}{\partial a} w_i^s \right) + J_{22}^{-1}\left(\sum_{i=1}^{n} \frac{\partial N_i}{\partial b} w_i^s \right) \end{aligned} \tag{10}$$

The first row of (10) represents the flexural contribution to the shear strain. Derived from the Kirchhoff part of the displacement field it is spurious if non-zero. The second row represents instead the genuine shear strain developed by the element under shearing effects. The shear strain can consequently be expressed as

$$\gamma_{yz} = \gamma_{yz}^b + \gamma_{yz}^s \tag{11}$$

where

$$\gamma_{yz}^b = J_{21}^{-1}\left(\sum_{i=1}^{n} \frac{\partial N_i}{\partial a} w_i^b \right) + J_{22}^{-1}\left(\sum_{i=1}^{n} \frac{\partial N_i}{\partial b} w_i^b \right) - \sum_{i=1}^{n} N_i \theta_i^b \tag{12}$$

$$\gamma_{yz}^s = J_{21}^{-1}\left(\sum_{i=1}^{n} \frac{\partial N_i}{\partial a} w_i^s \right) + J_{22}^{-1}\left(\sum_{i=1}^{n} \frac{\partial N_i}{\partial b} w_i^s \right) \tag{13}$$

Equation (11) allows the different contributions to shear strain to be identified and in particular allows the spurious shear strain to be explicitly expressed in (12).

The monomial test

As shown in (12) the spurious shear strain depends on the Kirchhoff field (w_i^b and θ_i^b) which is to be modelled by the element. The tendency of an element to lock can hence be investigated by checking the ability of the element to model specific displacement fields satisfying the Kirchhoff conditions in (5) (Briassoulis, 1988). A possible choice is a polynomial field given in the form of

$$w = \sum C_{pq} a^p b^q \tag{14}$$

where C_{pq} is a constant and p and q are non-negative integers. Displacement fields of this kind pass classical tests such as the ability to undergo rigid body motions and uniform strain which are traditionally utilised to highlight the influence of numerical integration, element distortion, mesh refinements and element order in the development of spurious shear strains and hence shear locking.

In particular the monomial test is applied in the following. The shear strain developed by the element is analysed when Kirchhoff fields in the form

$$w = C a^p b^q \tag{15}$$

are applied. By simply varying the values of the integer powers p and q, a full description of the flexural behaviour of the element is achieved.

As described in a previous research report (Eccher et al., 2005), the shape functions utilised in the isoparametric spline finite strip method are given by a combination of cubic Lagrangian one dimensional polynomials for the transverse direction and cubic B_3 spline series for the longitudinal direction.
The Lagrangian polynomials, which are function of the natural coordinate a, are expressed by

$$L_1(a) = -\frac{9}{16}\left(a^3 - a^2 - \frac{1}{9}a + \frac{1}{9}\right) \tag{16}$$

$$L_2(a) = \frac{27}{16}\left(a^3 - \frac{1}{3}a^2 - a + \frac{1}{3}\right) \tag{17}$$

$$L_3(a) = -\frac{27}{16}\left(a^3 + \frac{1}{3}a^2 - a - \frac{1}{3}\right) \tag{18}$$

$$L_4(a) = \frac{9}{16}\left(a^3 + a^2 - \frac{1}{9}a - \frac{1}{9}\right) \tag{19}$$

As shown in Fig. 1, the natural coordinate a is defined in the range [-1,1]. The first derivative of the Lagrangian functions (16), (17), (18) and (19) are given by

$$L_1'(a) = -\frac{27}{16}a^2 + \frac{9}{8}a + \frac{1}{16} \tag{20}$$

$$L_2'(a) = \frac{81}{16}a^2 - \frac{9}{8}a - \frac{27}{16} \tag{21}$$

$$L_3'(a) = -\frac{81}{16}a^2 - \frac{9}{8}a + \frac{27}{16} \tag{22}$$

$$L_4'(a) = \frac{27}{16}a^2 + \frac{9}{8}a - \frac{1}{16} \tag{23}$$

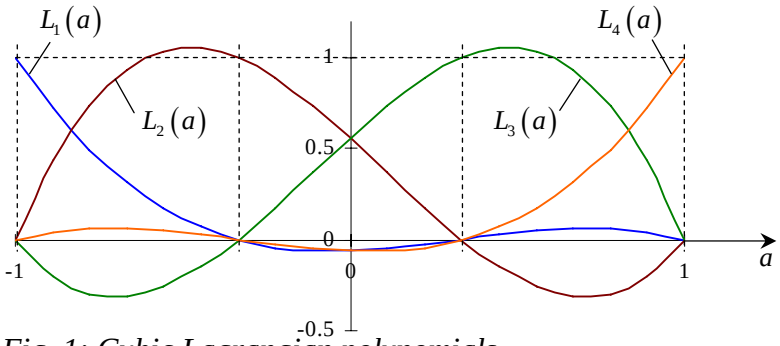

Fig. 1: Cubic Lagrangian polynomials.

Fig. 2 shows the generic j^{th} component of the B_3 spline series, which is a function of the natural coordinate $\tilde{b}$. The B_3 spline is a piecewise cubic polynomial given by

$$\tilde{\phi}_j\left(\tilde{b}\right) = \frac{1}{6}\begin{cases} 0 & , \tilde{b} < \tilde{b}_{j-2} \\ \left(\tilde{b} - \tilde{b}_{j-2}\right)^3 & , \tilde{b}_{j-2} \le \tilde{b} < \tilde{b}_{j-1} \\ 1 + 3\left(\tilde{b} - \tilde{b}_{j-1}\right) + 3\left(\tilde{b} - \tilde{b}_{j-1}\right)^2 - 3\left(\tilde{b} - \tilde{b}_{j-1}\right)^3 & , \tilde{b}_{j-1} \le \tilde{b} < \tilde{b}_j \\ 1 + 3\left(\tilde{b}_{j+1} - \tilde{b}\right) + 3\left(\tilde{b}_{j+1} - \tilde{b}\right)^2 - 3\left(\tilde{b}_{j+1} - \tilde{b}\right)^3 & , \tilde{b}_j \le \tilde{b} < \tilde{b}_{j+1} \\ \left(\tilde{b}_{j+2} - \tilde{b}\right)^3 & , \tilde{b}_{j+1} \le \tilde{b} < \tilde{b}_{j+2} \\ 0 & , \tilde{b} > \tilde{b}_{j+2} \end{cases} \tag{24}$$

where the natural coordinates, $\tilde{b}_j$, characterised by a subscript, j, are referred as to the nodal coordinates and assume the values of

$$\tilde{b}_j = j, \quad j = -1, 0, 1, \ldots, m+1 \tag{25}$$

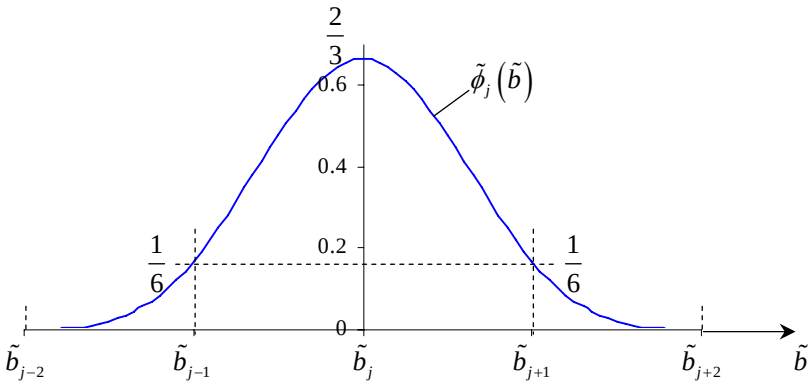

Fig. 2: Generic j^{th} B_3 spline component, $\tilde{\phi}_j(\tilde{b})$.

A complete B_3 spline series (Fig. 3) is characterised by m+3 B_3 spline components, (24), where m is referred to as the number of sections into which the strip is subdivided.

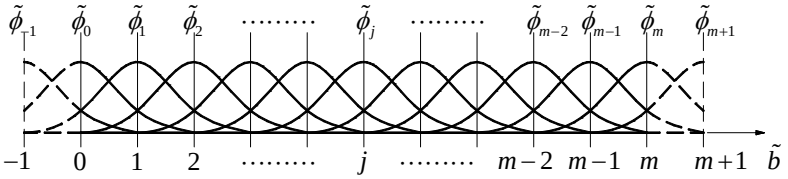

Fig. 3: Complete B_3 spline series, comprising m+3 components.

Without loosing the general validity of the demonstration and for ease of notation, we will here consider a strip characterised by a single section, i.e. m = 1. The full B_3 spline series (Fig. 4) is hence given by four components expressed by

$$\tilde{\phi}_{-1}(\tilde{b}) = \frac{1}{6}\left(1-\tilde{b}\right)^3 \tag{26}$$

$$\tilde{\phi}_0(\tilde{b}) = \frac{1}{6}\left(1+3\left(1-\tilde{b}\right)+3\left(1-\tilde{b}\right)^2-3\left(1-\tilde{b}\right)^3\right) \tag{27}$$

$$\tilde{\phi}_1(\tilde{b}) = \frac{1}{6}\left(1+3\tilde{b}+3\tilde{b}^2-3\tilde{b}^3\right) \tag{28}$$

$$\tilde{\phi}_2(\tilde{b}) = \frac{1}{6}\tilde{b}^3 \tag{29}$$

The natural coordinate $\tilde{b}$ is defined in the range [0,1] for a single section. It should be noticed that all non-zero sub-parts of the B_3 spline component, (24), are utilised. Their individual contributions to the development of spurious shear strains are hence taken into account.

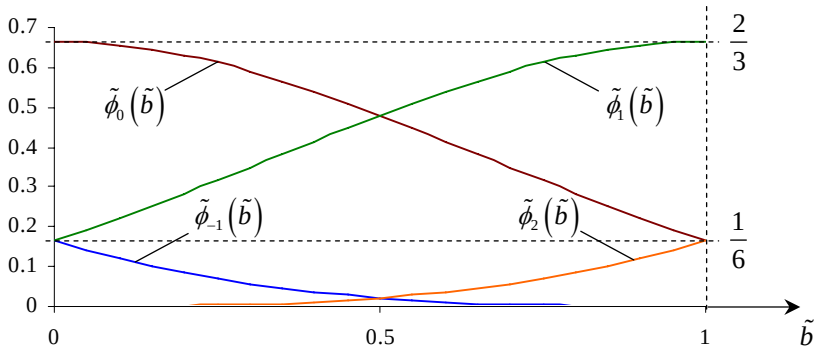

Fig. 4: Complete B_3 spline series when m = 1.

To help the understanding of the susceptibility of the isoparametric finite strip to locking, the spline functions given in (26)-(29) are mapped into the domain generally employed in the finite element method, i.e. [-1,1]. The mapping is performed by a linear coordinate transformation between the natural coordinate $\tilde{b}$ into the natural coordinate, b, in the [-1,1] domain (Fig. 5), i.e.

$$\tilde{b} = \frac{b+1}{2} \tag{30}$$

Substituting (30) in (26)-(29) we obtain

$$\tilde{\phi}_{-1}(b) = \frac{1}{48}(1-b)^3 \tag{31}$$

$$\tilde{\phi}_0(b) = \frac{1}{48}\left(23-15b-3b^2+3b^3\right) \tag{32}$$

$$\tilde{\phi}_1(b) = \frac{1}{48}\left(23+15b-3b^2-3b^3\right) \tag{33}$$

$$\tilde{\phi}_2(b) = \frac{1}{48}(1-b)^3 \tag{34}$$

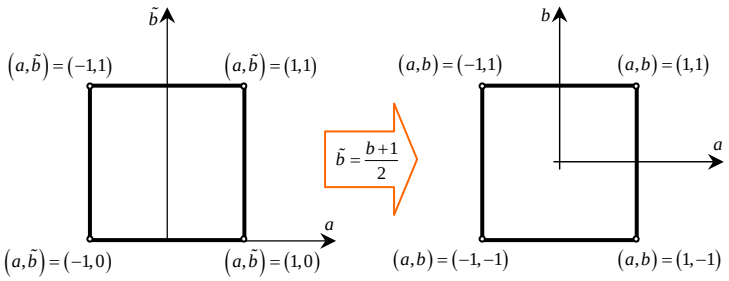

Fig. 5: Linear coordinate transformation.

The displacement functions are obtained by the following formula

$$\delta(a,b)=\sum_{i=1}^{4}\sum_{j=-1}^{2}L_i(a)\,\tilde{\phi}_j(b)\,\alpha_{ij}{}^{\delta} \tag{35}$$

where a and b are defined in [-1,1], $\delta(a,b)$ refers to the generic displacement field within the strip and $\alpha_{ij}{}^{\delta}$ is a set numerical coefficients related to the i^{th} nodal line and the j^{th} spline component. It should be noticed that the coefficients $\alpha_{ij}{}^{\delta}$ have no physical meaning, they are purely numerical coefficients.

For the purpose of applying the monomial test to the isoparametric spline finite strip, we have to relate the interpolating equation (35) to a generic Kirchhoff deflection field

$$w(a,b)=Ca^{p}b^{q} \tag{36}$$

and its associated rotation fields given by

$$\theta^{x}(a,b)=\frac{\partial w}{\partial x}=J_{11}^{-1}\frac{\partial w}{\partial a}+J_{12}^{-1}\frac{\partial w}{\partial b}=J_{11}^{-1}\theta^{a}(a,b)+J_{12}^{-1}\theta^{b}(a,b) \tag{37}$$

$$\theta^{y}(a,b)=\frac{\partial w}{\partial y}=J_{21}^{-1}\frac{\partial w}{\partial a}+J_{22}^{-1}\frac{\partial w}{\partial b}=J_{11}^{-1}\theta^{a}(a,b)+J_{12}^{-1}\theta^{b}(a,b) \tag{38}$$

where

$$\theta^{a}(a,b)=\frac{\partial w}{\partial a}=C\left(pa^{p-1}b^{q}\right) \tag{39}$$

$$\theta^{b}(a,b)=\frac{\partial w}{\partial b}=C\left(qa^{p}b^{q-1}\right) \tag{40}$$

It is easy to verify that the fields given in (36)-(40) yield zero shear strains, i.e.

$$\gamma_{xz}=\frac{\partial w}{\partial x}-\theta^{x}\equiv 0 \tag{41}$$

$$\gamma_{yz}=\frac{\partial w}{\partial y}-\theta^{y}\equiv 0 \tag{42}$$

The interpolated Kirchhoff field according to the isoparametric spline finite strip method is

$$w_s(a,b)=\sum_{i=1}^{4}\sum_{j=-1}^{2}L_i(a)\,\tilde{\phi}_j(b)\,\alpha_{ij}{}^{w} \tag{43}$$

$$\theta^{x}{}_{s}(a,b) = J_{11}^{-1}\theta^{a}{}_{s}(a,b) + J_{12}^{-1}\theta^{b}{}_{s}(a,b) \tag{44}$$

$$\theta^{y}{}_{s}(a,b) = J_{21}^{-1}\theta^{a}{}_{s}(a,b) + J_{22}^{-1}\theta^{b}{}_{s}(a,b) \tag{45}$$

where

$$\theta^{a}{}_{s}(a,b) = \sum_{i=1}^{4}\sum_{j=-1}^{2} L_i(a)\,\tilde{\phi}_j(b)\,\alpha_{ij}{}^{\theta^a} \tag{46}$$

$$\theta^{b}{}_{s}(a,b) = \sum_{i=1}^{4}\sum_{j=-1}^{2} L_i(a)\,\tilde{\phi}_j(b)\,\alpha_{ij}{}^{\theta^b} \tag{47}$$

It is clear that if the interpolated field coincides with the exact Kirchhoff field, i.e. if

$$w_s(a,b) \equiv w(a,b) \tag{48}$$

$$\theta^{a}{}_{s}(a,b) \equiv \theta^{a}(a,b) \tag{49}$$

$$\theta^{b}{}_{s}(a,b) \equiv \theta^{b}(a,b) \tag{50}$$

then the isoparametric spline finite strip method performs without developing spurious shear strain.

In what follows, we will prove that the conditions given in (48)-(50) are satisfied for Kirchhoff fields obtained by a combination of polynomials up to third order in both the natural coordinates *a* and *b*. Furthermore, we will prove that the spurious shear strains produced by the isoparametric spline finite strip formulation are zero at particular integration points, which differ from the reduced Gaussian integration points, in modelling Kirchhoff fields up to fourth order in both the natural coordinates *a* and *b*.

As mentioned in a previous research report (Eccher et al., 2005), the two extra spline components, ϕ_{-1} and ϕ_{m+1}, can be arbitrary associated with the values assumed by the displacement field or its derivatives at any point of the domain. By way of demonstration, we associate the spline coefficients with the values of the Kirchhoff field at the nodes of a grid defined by (i) the transverse natural coordinates, a_i, i.e.

$$a_1 \leftarrow a + 1 = 0 \tag{51}$$

$$a_2 \leftarrow a + \frac{1}{3} = 0 \tag{52}$$

$$a_3 \leftarrow a - \frac{1}{3} = 0 \tag{53}$$

$$a_4 \leftarrow a - 1 = 0 \tag{54}$$

and (ii) the longitudinal natural coordinates, b_j, i.e.

$$b_1 \leftarrow b+1=0 \tag{55}$$

$$b_2 \leftarrow b+\frac{1}{3}=0 \tag{56}$$

$$b_3 \leftarrow b-\frac{1}{3}=0 \tag{57}$$

$$b_4 \leftarrow b-1=0 \tag{58}$$

A graphical representation of the grid is given in Fig. 6.
Consequently, the sampling scheme can be expressed as follows:

$$w_s\left(a_i,b_j\right) \equiv w\left(a_i,b_j\right) = w_{ij}, \quad i,j=1,2,3,4 \tag{59}$$

$$\theta^a{}_s\left(a_i,b_j\right) \equiv \theta^a\left(a_i,b_j\right) = \theta^a{}_{ij}, \quad i,j=1,2,3,4 \tag{60}$$

$$\theta^b{}_s\left(a_i,b_j\right) \equiv \theta^b\left(a_i,b_j\right) = \theta^b{}_{ij}, \quad i,j=1,2,3,4 \tag{61}$$

Each one of (59)-(61) is a set of 16 independent equations establishing a unique relation between the spline coefficients, $\alpha_{ij}{}^{w}, \alpha_{ij}{}^{\theta^a}$ and $\alpha_{ij}{}^{\theta^b}$, and the values of the Kirchhoff field attained at the nodes of the grid, $w_{ij}, \theta^a{}_{ij}$ and $\theta^b{}_{ij}$, respectively.

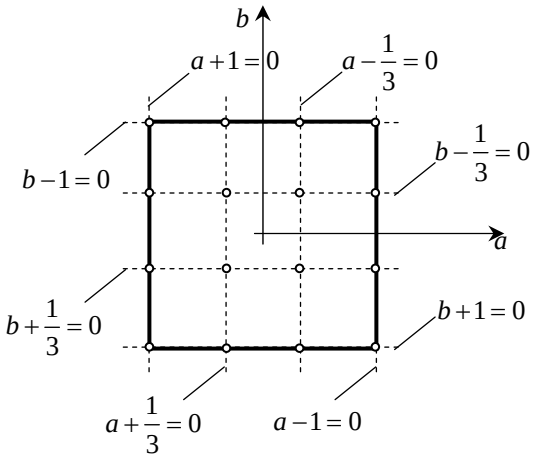

Fig. 6: Sampling points for the Lagrangian sampling scheme.

Concentrating on (59) and using (43) we have

$$w_s\left(a_i,b_j\right) = \sum_{k=1}^{4}\sum_{l=-1}^{2} L_k\left(a_i\right)\tilde{\phi}_l\left(b_j\right)\alpha_{kl}{}^{w} = w_{ij}, \quad i,j=1,2,3,4 \tag{62}$$

The contribution from the Lagrangian polynomials, $L_k(a_i)$, is identically zero unless $k = i$. Consequently, the system of 16 equations given in (62), uncouples into four sets of four equations, each given by

$$\left(w_s(a_i, b_j) = \sum_{l=-1}^{2} \tilde{\phi}_l(b_j) \alpha_{il}{}^{w} = w_{ij}, \quad j = 1,2 \ldots 4 \right), \quad i = 1,2,3,4 \tag{63}$$

The four independent linear systems of four equations given in (63) can be conveniently rewritten in matrix form as

$$\begin{bmatrix} \frac{1}{6} & \frac{2}{3} & \frac{1}{6} & 0 \\ \frac{4}{81} & \frac{31}{54} & \frac{10}{27} & \frac{1}{162} \\ \frac{1}{162} & \frac{10}{27} & \frac{4}{81} & \frac{4}{81} \\ 0 & \frac{1}{6} & \frac{2}{3} & \frac{1}{6} \end{bmatrix} \begin{bmatrix} \alpha^{w}_{i-1} \\ \alpha^{w}_{i0} \\ \alpha^{w}_{i1} \\ \alpha^{w}_{i2} \end{bmatrix} = \begin{bmatrix} w_{i1} \\ w_{i2} \\ w_{i3} \\ w_{i4} \end{bmatrix}, \quad i = 1,2,3,4 \tag{64}$$

Naming the coefficient matrix of (64) by **T**, i.e.

$$\mathbf{T} = \begin{bmatrix} \frac{1}{6} & \frac{2}{3} & \frac{1}{6} & 0 \\ \frac{4}{81} & \frac{31}{54} & \frac{10}{27} & \frac{1}{162} \\ \frac{1}{162} & \frac{10}{27} & \frac{4}{81} & \frac{4}{81} \\ 0 & \frac{1}{6} & \frac{2}{3} & \frac{1}{6} \end{bmatrix} \tag{65}$$

equation (64) can be rewritten as

$$\mathbf{T} \begin{bmatrix} \alpha^{w}_{i-1} \\ \alpha^{w}_{i0} \\ \alpha^{w}_{i1} \\ \alpha^{w}_{i2} \end{bmatrix} = \begin{bmatrix} w_{i1} \\ w_{i2} \\ w_{i3} \\ w_{i4} \end{bmatrix}, \quad i = 1,2,3,4 \tag{66}$$

Similar expressions can be obtained for the rotational components of the Kirchhoff field given in (60) and (61), i.e.

$$\mathbf{T}\begin{bmatrix} \alpha^{\theta^a}{}_{i-1} \\ \alpha^{\theta^a}{}_{i0} \\ \alpha^{\theta^a}{}_{i1} \\ \alpha^{\theta^a}{}_{i2} \end{bmatrix} = \begin{bmatrix} \theta^a{}_{i1} \\ \theta^a{}_{i2} \\ \theta^a{}_{i3} \\ \theta^a{}_{i4} \end{bmatrix}, \quad i = 1,2,3,4 \tag{67}$$

$$\mathbf{T}\begin{bmatrix} \alpha^{\theta^b}{}_{i-1} \\ \alpha^{\theta^b}{}_{i0} \\ \alpha^{\theta^b}{}_{i1} \\ \alpha^{\theta^b}{}_{i2} \end{bmatrix} = \begin{bmatrix} \theta^b{}_{i1} \\ \theta^b{}_{i2} \\ \theta^b{}_{i3} \\ \theta^b{}_{i4} \end{bmatrix}, \quad i = 1,2,3,4 \tag{68}$$

Furthermore, we note that the expression for the Kirchhoff deflection given in (43) can be rewritten as

$$\begin{aligned} w_s(a,b) &= \sum_{i=1}^{4}\sum_{j=-1}^{2} L_i(a)\,\tilde{\phi}_j(b)\,\alpha_{ij}{}^{w} \\ &= \sum_{i=1}^{4} L_i(a)\begin{bmatrix} \tilde{\phi}_{-1}(b) & \tilde{\phi}_0(b) & \tilde{\phi}_1(b) & \tilde{\phi}_2(b) \end{bmatrix}\begin{bmatrix} \alpha^{w}{}_{i-1} \\ \alpha^{w}{}_{i0} \\ \alpha^{w}{}_{i1} \\ \alpha^{w}{}_{i2} \end{bmatrix} \end{aligned} \tag{69}$$

By inverting the relation given in (66) and substituting it into (69) we obtain

$$w_s(a,b) = \sum_{i=1}^{4} L_i(a)\begin{bmatrix} \tilde{\phi}_{-1}(b) & \tilde{\phi}_0(b) & \tilde{\phi}_1(b) & \tilde{\phi}_2(b) \end{bmatrix}\mathbf{T}^{-1}\begin{bmatrix} w_{i1} \\ w_{i2} \\ w_{i3} \\ w_{i4} \end{bmatrix} \tag{70}$$

which can be rewritten as

$$w_s(a,b) = \sum_{i=1}^{4}\sum_{j=-1}^{2} L_i(a)\,\phi_j(b)\,w_{ij} \tag{71}$$

where we define

$$\begin{bmatrix} \phi_{-1}(b) & \phi_0(b) & \phi_1(b) & \phi_2(b) \end{bmatrix} = \begin{bmatrix} \tilde{\phi}_{-1}(b) & \tilde{\phi}_0(b) & \tilde{\phi}_1(b) & \tilde{\phi}_2(b) \end{bmatrix}\mathbf{T}^{-1} \tag{72}$$

It can be easily verified that for this specific interpolation scheme, the explicit form for the new $\phi_j(b)$ is

$$\phi_{-1}(b) = -\frac{9}{16}\cdot\left(b^3 - b^2 - \frac{1}{9}b + \frac{1}{9}\right) \tag{73}$$

$$\phi_0(b) = \frac{27}{16}\cdot\left(b^3 - \frac{1}{3}b^2 - b + \frac{1}{3}\right) \tag{74}$$

$$\phi_1(b) = -\frac{27}{16}\cdot\left(b^3 + \frac{1}{3}b^2 - b - \frac{1}{3}\right) \tag{75}$$

$$\phi_2(a) = \frac{9}{16}\cdot\left(b^3 + b^2 - \frac{1}{9}b - \frac{1}{9}\right) \tag{76}$$

and differentiating (73)-(76) with respect to the longitudinal natural coordinate, *b*, we get

$$\phi'_{-1}(b) = -\frac{27}{16}b^2 + \frac{9}{8}b + \frac{1}{16} \tag{77}$$

$$\phi'_0(b) = \frac{81}{16}b^2 - \frac{9}{8}b - \frac{27}{16} \tag{78}$$

$$\phi'_1(b) = -\frac{81}{16}b^2 - \frac{9}{8}b + \frac{27}{16} \tag{79}$$

$$\phi'_2(b) = \frac{27}{16}b^2 + \frac{9}{8}b - \frac{1}{16} \tag{80}$$

By comparing (73)-(80) with (16)-(23) we note that the new longitudinal functions, $\phi_j(b)$, are identical to the Lagrangian polynomials, $L_i(a)$, albeit in the *b* direction.

Similarly, for the other components of the Kirchhoff field we obtain

$$\theta^a{}_s(a,b) = \sum_{i=1}^{4}\sum_{j=-1}^{2} L_i(a)\,\phi_j(b)\,\theta^a{}_{ij} \tag{81}$$

$$\theta^b{}_s(a,b) = \sum_{i=1}^{4}\sum_{j=-1}^{2} L_i(a)\,\phi_j(b)\,\theta^b{}_{ij} \tag{82}$$

The sampled Kirchhoff field can now be explicitly evaluated by substituting the actual expressions for the coefficients w_{ij}, $\theta^a{}_{ij}$ and $\theta^b{}_{ij}$, i.e.

$$w_{ij} = Ca_i{}^p b_j{}^q \tag{83}$$

$$\theta^a{}_{ij} = pCa_i{}^{p-1} b_j{}^q \tag{84}$$

$$\theta^{b}{}_{ij} = qCa_i{}^{p} b_j{}^{q-1} \tag{85}$$

into (71), (81) and (82).

For the Kirchhoff field for the deflection, $w(a,b)$, we obtain an interpolated field, $w_s(a,b)$, given by:

- when both *p* and *q* are odd

$$\begin{aligned} w_s(a,b) = \Bigg[& \left(1-\left(\frac{1}{3}\right)^{p-1}-\left(\frac{1}{3}\right)^{q-1}+\left(\frac{1}{3}\right)^{p+q-2}\right)a^3b^3 + \\ & +\left(-\left(\frac{1}{3}\right)^{2}+\left(\frac{1}{3}\right)^{p+1}+\left(\frac{1}{3}\right)^{q-1}-\left(\frac{1}{3}\right)^{p+q-2}\right)a^3b + \\ & +\left(-\left(\frac{1}{3}\right)^{2}+\left(\frac{1}{3}\right)^{p-1}+\left(\frac{1}{3}\right)^{q+1}-\left(\frac{1}{3}\right)^{p+q-2}\right)ab^3 + \\ & +\left(\left(\frac{1}{3}\right)^{4}-\left(\frac{1}{3}\right)^{p+1}-\left(\frac{1}{3}\right)^{q+1}+\left(\frac{1}{3}\right)^{p+q-2}\right)ab\Bigg]\frac{81}{64}C \end{aligned} \tag{86}$$

- when *p* is odd and *q* is even

$$\begin{aligned} w_s(a,b) = \Bigg[& \left(1-\left(\frac{1}{3}\right)^{p-1}-\left(\frac{1}{3}\right)^{q}+\left(\frac{1}{3}\right)^{p+q-1}\right)a^3b^2 + \\ & +\left(-\left(\frac{1}{3}\right)^{2}+\left(\frac{1}{3}\right)^{p+1}+\left(\frac{1}{3}\right)^{q}-\left(\frac{1}{3}\right)^{p+q-1}\right)a^3 + \\ & +\left(-\left(\frac{1}{3}\right)^{2}+\left(\frac{1}{3}\right)^{p-1}+\left(\frac{1}{3}\right)^{q+2}-\left(\frac{1}{3}\right)^{p+q-1}\right)ab^2 + \\ & +\left(\left(\frac{1}{3}\right)^{4}-\left(\frac{1}{3}\right)^{p+1}-\left(\frac{1}{3}\right)^{q+2}+\left(\frac{1}{3}\right)^{p+q-1}\right)a\Bigg]\frac{81}{64}C \end{aligned} \tag{87}$$

- when *p* is even and *q* is odd

$$
\begin{aligned}
w_s(a,b) = \Bigg[& \left(1-\left(\frac{1}{3}\right)^{p}-\left(\frac{1}{3}\right)^{q-1}+\left(\frac{1}{3}\right)^{p+q-1}\right)a^2b^3 + \\
& +\left(-\left(\frac{1}{3}\right)^{2}+\left(\frac{1}{3}\right)^{p+2}+\left(\frac{1}{3}\right)^{q-1}-\left(\frac{1}{3}\right)^{p+q-1}\right)a^2b + \\
& +\left(-\left(\frac{1}{3}\right)^{2}+\left(\frac{1}{3}\right)^{p}+\left(\frac{1}{3}\right)^{q+1}-\left(\frac{1}{3}\right)^{p+q-1}\right)b^3 + \\
& +\left(\left(\frac{1}{3}\right)^{4}-\left(\frac{1}{3}\right)^{p+2}-\left(\frac{1}{3}\right)^{q+1}+\left(\frac{1}{3}\right)^{p+q-1}\right)b\Bigg]\frac{81}{64}C
\end{aligned}
\tag{88}
$$

- when both *p* and *q* are even

$$
\begin{aligned}
w_s(a,b) = \Bigg[& \left(1-\left(\frac{1}{3}\right)^{p}-\left(\frac{1}{3}\right)^{q}+\left(\frac{1}{3}\right)^{p+q}\right)a^2b^2 + \\
& +\left(-\left(\frac{1}{3}\right)^{2}+\left(\frac{1}{3}\right)^{p+2}+\left(\frac{1}{3}\right)^{q}-\left(\frac{1}{3}\right)^{p+q}\right)a^2 + \\
& +\left(-\left(\frac{1}{3}\right)^{2}+\left(\frac{1}{3}\right)^{p}+\left(\frac{1}{3}\right)^{q+2}-\left(\frac{1}{3}\right)^{p+q}\right)b^2 + \\
& +\left(\left(\frac{1}{3}\right)^{4}-\left(\frac{1}{3}\right)^{p+2}-\left(\frac{1}{3}\right)^{q+2}+\left(\frac{1}{3}\right)^{p+q}\right)\Bigg]\frac{81}{64}C
\end{aligned}
\tag{89}
$$

By inspection of equations (86)-(89) one can verify that the isoparametric spline finite strip method is able to exactly reproduce any Kirchhoff deflection field, $w(a,b)$, given by a complete polynomial up to the third power in both the transverse natural coordinate, *a*, and the longitudinal natural coordinate, *b*, i.e. for any Kirchhoff field given in (36) with *p* and *q* less than or equal to three.

For the rotational Kirchhoff field $\theta^a(a,b)$, we obtain a sampled field, $\theta^a{}_s(a,b)$, given by:

- when *p* is even and *q* is odd

$$\theta_s^a(a,b)=\left[\left(1-\left(\frac{1}{3}\right)^{p-2}-\left(\frac{1}{3}\right)^{q-1}+\left(\frac{1}{3}\right)^{p+q-3}\right)a^3b^3+\right.$$
$$+\left(-\left(\frac{1}{3}\right)^{2}+\left(\frac{1}{3}\right)^{p}+\left(\frac{1}{3}\right)^{q-1}-\left(\frac{1}{3}\right)^{p+q-3}\right)a^3b+$$
$$+\left(-\left(\frac{1}{3}\right)^{2}+\left(\frac{1}{3}\right)^{p-2}+\left(\frac{1}{3}\right)^{q+1}-\left(\frac{1}{3}\right)^{p+q-3}\right)ab^3+$$
$$\left.+\left(\left(\frac{1}{3}\right)^{4}-\left(\frac{1}{3}\right)^{p}-\left(\frac{1}{3}\right)^{q+1}+\left(\frac{1}{3}\right)^{p+q-3}\right)ab\right]\frac{81}{64}pC \tag{90}$$

- when both p and q are even

$$\theta_s^a(a,b)=\left[\left(1-\left(\frac{1}{3}\right)^{p-2}-\left(\frac{1}{3}\right)^{q}+\left(\frac{1}{3}\right)^{p+q-2}\right)a^3b^2+\right.$$
$$+\left(-\left(\frac{1}{3}\right)^{2}+\left(\frac{1}{3}\right)^{p}+\left(\frac{1}{3}\right)^{q}-\left(\frac{1}{3}\right)^{p+q-2}\right)a^3+$$
$$+\left(-\left(\frac{1}{3}\right)^{2}+\left(\frac{1}{3}\right)^{p-2}+\left(\frac{1}{3}\right)^{q+2}-\left(\frac{1}{3}\right)^{p+q-2}\right)ab^2+$$
$$\left.+\left(\left(\frac{1}{3}\right)^{4}-\left(\frac{1}{3}\right)^{p}-\left(\frac{1}{3}\right)^{q+2}+\left(\frac{1}{3}\right)^{p+q-2}\right)a\right]\frac{81}{64}pC \tag{91}$$

- when both p and q are odd

$$\theta_s^a(a,b)=\left[\left(1-\left(\frac{1}{3}\right)^{p-1}-\left(\frac{1}{3}\right)^{q-1}+\left(\frac{1}{3}\right)^{p+q-2}\right)a^2b^3+\right.$$
$$+\left(-\left(\frac{1}{3}\right)^{2}+\left(\frac{1}{3}\right)^{p+1}+\left(\frac{1}{3}\right)^{q-1}-\left(\frac{1}{3}\right)^{p+q-2}\right)a^2b+$$
$$+\left(-\left(\frac{1}{3}\right)^{2}+\left(\frac{1}{3}\right)^{p-1}+\left(\frac{1}{3}\right)^{q+1}-\left(\frac{1}{3}\right)^{p+q-2}\right)b^3+$$
$$\left.+\left(\left(\frac{1}{3}\right)^{4}-\left(\frac{1}{3}\right)^{p+1}-\left(\frac{1}{3}\right)^{q+1}+\left(\frac{1}{3}\right)^{p+q-2}\right)b\right]\frac{81}{64}pC \tag{92}$$

- when p is odd and q is even

$$\theta_s^a(a,b)=\left[\left(1-\left(\frac{1}{3}\right)^{p-1}-\left(\frac{1}{3}\right)^{q}+\left(\frac{1}{3}\right)^{p+q-1}\right)a^2b^2+\right.$$
$$+\left(-\left(\frac{1}{3}\right)^{2}+\left(\frac{1}{3}\right)^{p+1}+\left(\frac{1}{3}\right)^{q}-\left(\frac{1}{3}\right)^{p+q-1}\right)a^2+$$
$$+\left(-\left(\frac{1}{3}\right)^{2}+\left(\frac{1}{3}\right)^{p-1}+\left(\frac{1}{3}\right)^{q+2}-\left(\frac{1}{3}\right)^{p+q-1}\right)b^2+$$
$$\left.+\left(\left(\frac{1}{3}\right)^{4}-\left(\frac{1}{3}\right)^{p+1}-\left(\frac{1}{3}\right)^{q+2}+\left(\frac{1}{3}\right)^{p+q-1}\right)\right]\frac{81}{64}pC \tag{93}$$

By inspection of equations (90)-(93) one can verify that the isoparametric spline finite strip method is able to exactly reproduce any Kirchhoff rotational field, $\theta^a(a,b)$, related to a displacement Kirchhoff field, $w(a,b)$, given by a complete polynomial up to fourth power in the transverse natural coordinate, *a*, and up to third power in the longitudinal natural coordinate, *b*, i.e. for any Kirchhoff field given in (36) with *p* less than or equal to four and *q* less than or equal to three.

For the rotational Kirchhoff field $\theta^b(a,b)$, we obtain a sampled field, $\theta^b{}_s(a,b)$, given by:

- when *p* is odd and *q* is even

$$\theta_s^b(a,b)=\left[\left(1-\left(\frac{1}{3}\right)^{p-1}-\left(\frac{1}{3}\right)^{q-2}+\left(\frac{1}{3}\right)^{p+q-3}\right)a^3b^3+\right.$$
$$+\left(-\left(\frac{1}{3}\right)^{2}+\left(\frac{1}{3}\right)^{p+1}+\left(\frac{1}{3}\right)^{q-2}-\left(\frac{1}{3}\right)^{p+q-3}\right)a^3b+$$
$$+\left(-\left(\frac{1}{3}\right)^{2}+\left(\frac{1}{3}\right)^{p-1}+\left(\frac{1}{3}\right)^{q}-\left(\frac{1}{3}\right)^{p+q-3}\right)ab^3+$$
$$\left.+\left(\left(\frac{1}{3}\right)^{4}-\left(\frac{1}{3}\right)^{p+1}-\left(\frac{1}{3}\right)^{q}+\left(\frac{1}{3}\right)^{p+q-3}\right)ab\right]\frac{81}{64}qC \tag{94}$$

- when both *p* and *q* are odd

$$\theta_s^b(a,b)=\left[\left(1-\left(\frac{1}{3}\right)^{p-1}-\left(\frac{1}{3}\right)^{q-1}+\left(\frac{1}{3}\right)^{p+q-2}\right)a^3b^2+\right.$$
$$+\left(-\left(\frac{1}{3}\right)^{2}+\left(\frac{1}{3}\right)^{p+1}+\left(\frac{1}{3}\right)^{q-1}-\left(\frac{1}{3}\right)^{p+q-2}\right)a^3+$$
$$+\left(-\left(\frac{1}{3}\right)^{2}+\left(\frac{1}{3}\right)^{p-1}+\left(\frac{1}{3}\right)^{q+1}-\left(\frac{1}{3}\right)^{p+q-2}\right)ab^2+$$
$$\left.+\left(\left(\frac{1}{3}\right)^{4}-\left(\frac{1}{3}\right)^{p+1}-\left(\frac{1}{3}\right)^{q+1}+\left(\frac{1}{3}\right)^{p+q-2}\right)a\right]\frac{81}{64}qC \tag{95}$$

- when both p and q are even

$$\theta_s^b(a,b)=\left[\left(1-\left(\frac{1}{3}\right)^{p}-\left(\frac{1}{3}\right)^{q-2}+\left(\frac{1}{3}\right)^{p+q-2}\right)a^2b^3+\right.$$
$$+\left(-\left(\frac{1}{3}\right)^{2}+\left(\frac{1}{3}\right)^{p+2}+\left(\frac{1}{3}\right)^{q-2}-\left(\frac{1}{3}\right)^{p+q-2}\right)a^2b+$$
$$+\left(-\left(\frac{1}{3}\right)^{2}+\left(\frac{1}{3}\right)^{p}+\left(\frac{1}{3}\right)^{q}-\left(\frac{1}{3}\right)^{p+q-2}\right)b^3+$$
$$\left.+\left(\left(\frac{1}{3}\right)^{4}-\left(\frac{1}{3}\right)^{p+2}-\left(\frac{1}{3}\right)^{q}+\left(\frac{1}{3}\right)^{p+q-2}\right)b\right]\frac{81}{64}qC \tag{96}$$

- when p is even and q is odd

$$\theta_s^b(a,b)=\left[\left(1-\left(\frac{1}{3}\right)^{p}-\left(\frac{1}{3}\right)^{q-1}+\left(\frac{1}{3}\right)^{p+q-1}\right)a^2b^2+\right.$$
$$+\left(-\left(\frac{1}{3}\right)^{2}+\left(\frac{1}{3}\right)^{p+2}+\left(\frac{1}{3}\right)^{q-1}-\left(\frac{1}{3}\right)^{p+q-1}\right)a^2+$$
$$+\left(-\left(\frac{1}{3}\right)^{2}+\left(\frac{1}{3}\right)^{p}+\left(\frac{1}{3}\right)^{q+1}-\left(\frac{1}{3}\right)^{p+q-1}\right)b^2+$$
$$\left.+\left(\left(\frac{1}{3}\right)^{4}-\left(\frac{1}{3}\right)^{p+2}-\left(\frac{1}{3}\right)^{q+1}+\left(\frac{1}{3}\right)^{p+q-1}\right)\right]\frac{81}{64}qC \tag{97}$$

It follows from equations (94)-(97) that the isoparametric spline finite strip method is able to exactly reproduce any Kirchhoff rotational field, $\theta^b(a,b)$, related to a displacement Kirchhoff field, $w(a,b)$, given by a complete polynomial up to third power in the transverse natural coordinate, *a*, and up to fourth power in the longitudinal natural coordinate, *b*, i.e. for any Kirchhoff field given in (36) with *p* less than or equal to three and *q* less than or equal to four.

By combining the results obtained in equations (86)-(97) we have proved that the isoparametric spline finite strip method can exactly interpolate a Kirchhoff field up to the third power in both the transverse natural coordinate, *a*, and the longitudinal natural coordinate, *b*. As previously stated, this ensures that no spurious shear strain is developed by the isoparametric spline finite strip method for Kirchhoff fields having the form

$$\begin{aligned} w_1(a,b) = C_0 + C_1 a + C_2 b + C_3 ab + C_4 a^2 + C_5 b^2 + C_6 a^2 b + C_7 ab^2 + C_8 a^2 b^2 + \\ + C_9 a^3 + C_{10} b^3 + C_{11} a^3 b + C_{12} ab^3 + C_{13} a^3 b^2 + C_{14} a^2 b^3 + C_{15} a^3 b^3 \end{aligned} \tag{98}$$

regardless of the integration scheme and the distortion of the strip.

Furthermore, to investigate the performance of the isoparametric spline finite strip with regard to higher order Kirchhoff fields, we may write the expression for the spurious shear strains obtained by the isoparametric spline finite strip sampling, $\left(\gamma_{xz}(a,b)\right)_s$ and $\left(\gamma_{yz}(a,b)\right)_s$, as

$$\begin{aligned} \gamma_{xz} &= \frac{\partial w}{\partial x} - \theta^x \\ &= CJ_{11}^{-1} \sum_{i=1}^{4} \sum_{j=-1}^{2} \left(L_i' \, \phi_j \, a_i^p b_j^q - q\left(L_i \, \phi_j \, a_i^p b_j^{q-1} \right) \right) + \\ &+ CJ_{12}^{-1} \sum_{i=1}^{n} \left(L_i \, \phi_j' \, a_i^p b_j^q - p\left(L_i \, \phi_j \, a_i^{p-1} b_j^q \right) \right) \end{aligned} \tag{99}$$

$$\begin{aligned} \gamma_{yz} &= \frac{\partial w}{\partial y} - \theta^y \\ &= CJ_{21}^{-1} \sum_{i=1}^{4} \sum_{j=-1}^{2} \left(L_i' \, \phi_j \, a_i^p b_j^q - q\left(L_i \, \phi_j \, a_i^p b_j^{q-1} \right) \right) + \\ &+ CJ_{22}^{-1} \sum_{i=1}^{n} \left(L_i \, \phi_j' \, a_i^p b_j^q - p\left(L_i \, \phi_j \, a_i^{p-1} b_j^q \right) \right) \end{aligned} \tag{100}$$

By evaluating (99) and (100) for *p* equal to four and *q* less than or equal to three, we obtain spurious shear strains given by

$$\gamma_{xz}(a,b) = -\frac{4}{9} C J_{11}^{-1} a\left(9a^2 - 5\right) b^q \tag{101}$$

$$\gamma_{yz}(a,b) = -\frac{4}{9} C J_{21}^{-1} a\left(9a^2 - 5\right) b^q \tag{102}$$

Similarly, for Kirchhoff fields up to third power in the transverse natural coordinate, *a*, i.e. for *p* less than or equal to three, and of fourth power in the longitudinal natural coordinate, *b* , i.e. for *q* equal to four, we obtain spurious shear strains given by

$$\gamma_{xz}(a,b) = -\frac{4}{9} C J_{11}^{-1} a^p b\left(9b^2 - 5\right) \tag{103}$$

$$\gamma_{yz}(a,b) = -\frac{4}{9} C J_{21}^{-1} a^p b\left(9b^2 - 5\right) \tag{104}$$

Finally, if we evaluate the spurious shear strain produced by the isoparametric spline finite strip method, subjected to a Kirchhoff field of fourth power in both the natural coordinate *a* and *b*, i.e. for *p* and *q* equal to four, we obtain

$$\gamma_{xz}(a,b) = -\frac{4}{81} C\left(J_{11}^{-1} a\left(9a^2 - 5\right)\left(10b^2 - 1\right) + J_{12}^{-1}\left(10a^2 - 1\right) b\left(9b^2 - 5\right)\right) \tag{105}$$

$$\gamma_{yz}(a,b) = -\frac{4}{81} C\left(J_{11}^{-1} a\left(9a^2 - 5\right)\left(10b^2 - 1\right) + J_{12}^{-1}\left(10a^2 - 1\right) b\left(9b^2 - 5\right)\right) \tag{106}$$

We note that, the spurious shear strains expressed by (101)-(106) equal zero when evaluated at the nodes of the grid shown in Fig. 7, given by the following lines

$$a + \frac{\sqrt{5}}{3} = 0 \tag{107}$$

$$a = 0 \tag{108}$$

$$a - \frac{\sqrt{5}}{3} = 0 \tag{109}$$

$$b + \frac{\sqrt{5}}{3} = 0 \tag{110}$$

$$b = 0 \tag{111}$$

$$b - \frac{\sqrt{5}}{3} = 0 \tag{112}$$

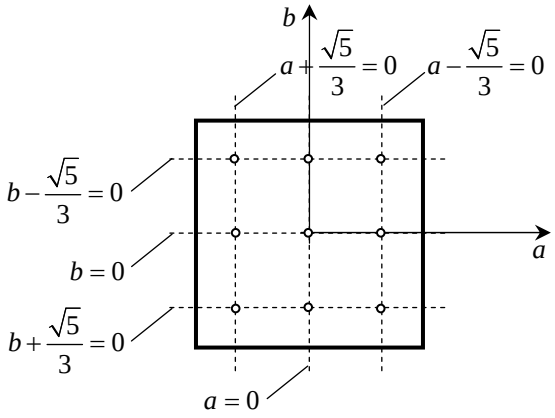

Fig. 7: Modified reduced integration points for the Lagrangian sampling scheme.

This suggest that if a reduced integration is performed on the nodes of the grid given by (107)-(112), the isoparametric spline finite strip is able to perform without developing spurious shear strain under local Kirchhoff fields given by a combination of terms up to fourth order in both the natural coordinates, *a* and *b*. In addition to the Kirchhoff field given in (98), under modified reduced integration, the isoparametric spline finite strip also produces no spurious shear strain for fields having the form

$$w_2(a,b) = C_{16}a^4 + C_{17}b^4 + C_{18}a^4b + C_{19}ab^4 + C_{20}a^4b^2 + \\ + C_{21}a^2b^4 + C_{22}a^4b^3 + C_{23}a^3b^4 + C_{24}a^4b^4 \tag{113}$$

provided the integration points are chosen as shown in Fig. 7.

It is important to notice that the choice of interpolation points to be used with the isoparametric spline finite strip method (see (51)-(58)) does not alter the above derivations. Regardless of the sampling scheme adopted in defining the Kirchhoff field, the isoparametric spline finite strip is able to perform without developing spurious shear strains, under Kirchhoff fields up to third order given by (98). In addition to the field in (98), Kirchhoff fields of the form given by (113) can also be reproduced by the isoparametric spline finite strip if a modified selective reduced integration technique is adopted.

A different choice of sampling points alters the expression for the longitudinal functions, $\phi_j(b)$ and, consequently, the location of the optimal reduced integration points. Following the same procedure described in the previous sections, we summarise here the results obtained with two other possible sampling schemes.

Choosing firstly a sampling scheme given by the nodes of the grid shown in Fig. 8, defined by the lines

$$a + 1 = 0 \tag{114}$$

$$a + \frac{1}{3} = 0 \tag{115}$$

$$a-\frac{1}{3}=0 \tag{116}$$

$$a-1=0 \tag{117}$$

$$b+1=0 \tag{118}$$

$$b+\frac{1}{2}=0 \tag{119}$$

$$b-\frac{1}{2}=0 \tag{120}$$

$$b-1=0 \tag{121}$$

we obtain a set of longitudinal functions $\phi_j(b)$ given by

$$\phi_{-1}(b)=-\frac{2}{3}\left(b^3-b^2-\frac{1}{4}b+\frac{1}{4}\right) \tag{122}$$

$$\phi_0(b)=\frac{2}{3}\left(2b^3-b^2-2b+1\right) \tag{123}$$

$$\phi_1(b)=-\frac{2}{3}\left(2b^3+b^2-2b-1\right) \tag{124}$$

$$\phi_2(a)=\frac{2}{3}\left(b^3+b^2-\frac{1}{4}b-\frac{1}{4}\right) \tag{125}$$

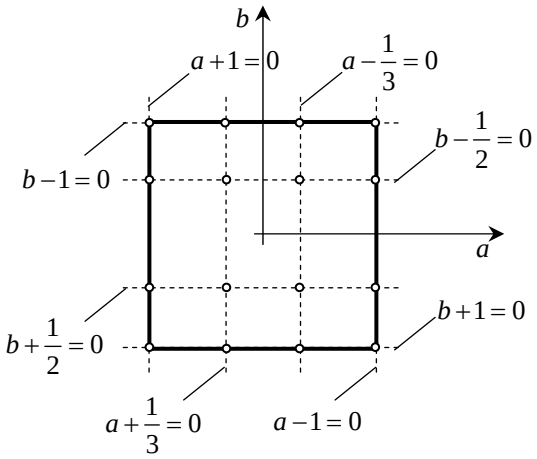

Fig. 8: Sampling points for a different sampling scheme.

By inserting the new longitudinal functions (122)-(125) and their derivatives in (99) and (100) we obtain spurious shear strains that for a Kirchhoff fields of fourth order in the transverse natural coordinate, *a*, and up to third order in the longitudinal natural coordinate, *b*, are given by

$$\gamma_{xz}(a,b)=-\frac{4}{9}CJ_{11}^{-1}a\left(9a^2-5\right)b^q \tag{126}$$

$$\gamma_{yz}(a,b) = -\frac{4}{9} C J_{21}^{-1} a\left(9a^2 - 5\right) b^q \tag{127}$$

Similarly, for Kirchhoff fields up to third power in the transverse natural coordinate, *a*, i.e. for *p* less than or equal to three, and of fourth power in the longitudinal natural coordinate, *b* , i.e. for *q* equal to four, we obtain spurious shear strains given by

$$\gamma_{xz}(a,b) = -\frac{1}{2} C J_{12}^{-1} a^p b\left(8b^2 - 5\right) \tag{128}$$

$$\gamma_{yz}(a,b) = -\frac{1}{2} C J_{22}^{-1} a^p b\left(8b^2 - 5\right) \tag{129}$$

Finally, if we evaluate the spurious shear strain produced by the isoparametric spline finite strip method, subjected to a Kirchhoff field of fourth power in both the natural coordinate *a* and *b*, i.e. for *p* and *q* equal to four, we obtain

$$\gamma_{xz}(a,b) = -\frac{1}{18} C\left(2J_{11}^{-1} a\left(9a^2 - 5\right)\left(5b^2 - 1\right) + J_{12}^{-1}\left(10a^2 - 1\right) b\left(8b^2 - 5\right)\right) \tag{130}$$

$$\gamma_{yz}(a,b) = -\frac{1}{18} C\left(2J_{21}^{-1} a\left(9a^2 - 5\right)\left(5b^2 - 1\right) + J_{22}^{-1}\left(10a^2 - 1\right) b\left(8b^2 - 5\right)\right) \tag{131}$$

We observe that the spurious shear strains expressed by (126)-(131) equal zero when evaluated at the nodes of the grid given in Fig. 9 and expressed by the following lines

$$a + \frac{\sqrt{5}}{3} = 0 \tag{132}$$

$$a = 0 \tag{133}$$

$$a - \frac{\sqrt{5}}{3} = 0 \tag{134}$$

$$b + \sqrt{\frac{5}{8}} = 0 \tag{135}$$

$$b = 0 \tag{136}$$

$$b - \sqrt{\frac{5}{8}} = 0 \tag{137}$$

This suggest that if reduced integration is performed on the nodes of the grid given by (132)-(137), the isoparametric spline finite strip is again able to perform without developing spurious shear strain for the fourth order local Kirchhoff field given by (113).

Another possible choice for the sampling technique is to sample the components of the Kirchhoff field, $w(a,b)$, $\theta^a(a,b)$ and $\theta^b(a,b)$, as well as their derivatives with respect to the longitudinal natural coordinate, *b*, at the nodes of the grid shown in Fig. 10 and given by the lines

$$a+1=0 \tag{138}$$
$$a+\frac{1}{3}=0 \tag{139}$$
$$a-\frac{1}{3}=0 \tag{140}$$
$$a-1=0 \tag{141}$$
$$b+1=0 \tag{142}$$
$$b-1=0 \tag{143}$$

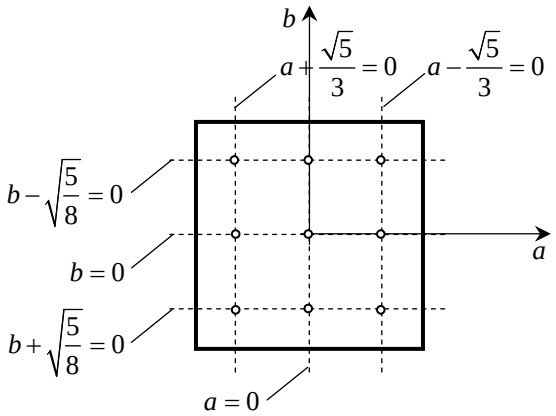

Fig. 9: Modified reduced integration points for a different sampling scheme.

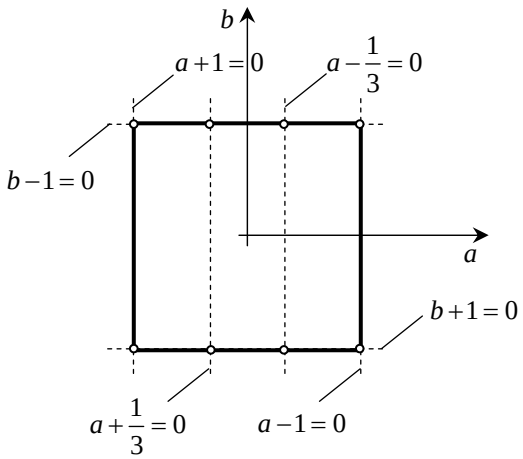

Fig. 10: Sampling points for a displacement and rotations sampling scheme.

This particular choice for the sampling points produces a set of longitudinal functions $\phi_j(b)$ given by

$$\phi_{-1}(b)=\frac{1}{4}\left(b^3-b^2-b+1\right) \tag{144}$$

$$\phi_{0}(b)=\frac{1}{4}\left(b^3-3b+2\right) \tag{145}$$

$$\phi_{1}(b)=-\frac{1}{4}\left(b^3-3b-2\right) \tag{146}$$

$$\phi_{2}(a)=\frac{1}{4}\left(b^3+b^2-b-1\right) \tag{147}$$

These functions are the cubic Hermite polynomials. According to this interpolation scheme, the spurious shear strains produced by Kirchhoff fields of fourth order in the transverse natural coordinate, *a*, and up to third order in the longitudinal natural coordinate, *b*, are given by

$$\gamma_{xz}(a,b)=-\frac{4}{9}CJ_{11}^{-1}a\left(9a^2-5\right)b^q \tag{148}$$

$$\gamma_{yz}(a,b)=-\frac{4}{9}CJ_{21}^{-1}a\left(9a^2-5\right)b^q \tag{149}$$

Similarly, for Kirchhoff fields up to third order in the transverse natural coordinate, *a*, i.e. for *p* less than or equal to three, and of fourth order in the longitudinal natural coordinate, *b* , i.e. for *q* equal to four, we obtain spurious shear strains given by

$$\gamma_{xz}(a,b)=-4CJ_{12}^{-1}a^p b(b-1)(b+1) \tag{150}$$

$$\gamma_{yz}(a,b)=-4CJ_{22}^{-1}a^p b(b-1)(b+1) \tag{151}$$

Finally, if we evaluate the spurious shear strain produced by the isoparametric spline finite strip method, subjected to a Kirchhoff field of fourth order in both the natural coordinate *a* and *b*, i.e. for *p* and *q* equal to four, we obtain

$$\gamma_{xz}(a,b)=-\frac{4}{9}C\left(J_{11}^{-1}a\left(9a^2-5\right)\left(2b^2-1\right)+J_{12}^{-1}\left(10a^2-1\right)b(b-1)(b+1)\right) \tag{152}$$

$$\gamma_{yz}(a,b)=-\frac{4}{9}C\left(J_{21}^{-1}a\left(9a^2-5\right)\left(2b^2-1\right)+J_{22}^{-1}\left(10a^2-1\right)b(b-1)(b+1)\right) \tag{153}$$

We observe that the spurious shear strains expressed by (148)-(153) equal zero when evaluated at the nodes of the grid shown in Fig. 11 and given by the following lines

$$a+\frac{\sqrt{5}}{3}=0 \tag{154}$$

$$a=0 \tag{155}$$

$$a-\frac{\sqrt{5}}{3}=0 \tag{156}$$

$$b+1=0 \tag{157}$$

$$b=0 \tag{158}$$

$$b-1=0 \tag{159}$$

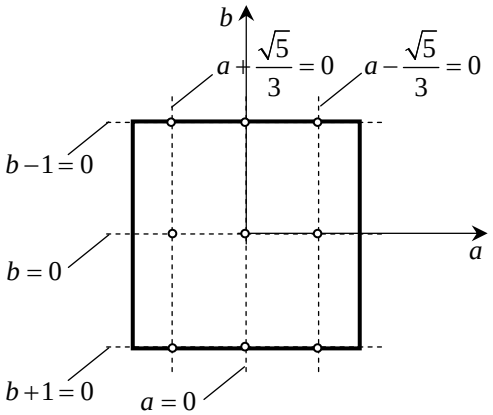

Fig. 11: Modified reduced integration points for the Hermite sampling scheme.

This suggest that if a reduced integration is performed on the nodes of the grid given by (154)-(159), the isoparametric spline finite strip is able to perform without developing spurious shear strain for the fourth order local Kirchhoff field given (113).

Integration scheme and strip distortion

The previous considerations were concerned with identifying integration points that would eliminate spurious shear strains for various orders of Kirchhoff fields. Unfortunately, if integration points different from the Gaussian points are used, the accuracy of the numerical integration decreases. The Gaussian integration points are optimal for performing an exact integration of polynomials of order less than $2n$, where n is the number of integration points. By fixing a certain number, n_{fix}, of integration points, the accuracy of the numerical integration decreases and only polynomials of order less than $2n\text{-}n_{fix}$ can be exactly integrated. In this particular case, n is equal to three and the integration points, n_{fix}, fixed in order to avoid shear locking, is two. Consequently, the numerical integration is able to exactly integrate polynomials of less than fourth order, while the polynomials involved in the integration of the shear components of the stiffness matrix are of higher order.

In terms of spurious contributions to the total potential energy of the finite strip, the error introduced by the inaccuracy of the integration scheme is greater than the error introduced by integrating the shear contribution to the stiffness matrix at the reduced Gaussian integration points, where the spurious shear strain is not zero. To illustrate this result, the performance of the isoparametric spline finite strip is analysed by varying the geometrical distortion of the strip and the integration scheme.

The method proposed in a previous report (Eccher et all., 2005) transforms the two nodal coefficients at the extremes of each nodal line, α_{i-1}, α_{i0} and α_{im}, α_{im+1}, into the nodal values of the generic displacement function, δ_{i0} and δ_{im}, and the first derivative of the displacement with respect to the global longitudinal *y* coordinate, $\partial\delta/\partial y_{i0}$ and $\partial\delta/\partial y_{im}$. This particular transformation allows an appropriate assembly of the strips in the longitudinal direction. The derivation of the new longitudinal functions, $\phi_j(b)$, for this particular sampling scheme is rather more complex than the previous cases and we will report here only the results obtained in terms of the spurious shear strains expressions.

The spurious shear strains produced by Kirchhoff fields of fourth order in the transverse natural coordinate, *a*, and up to third order in the longitudinal natural coordinate, *b*, are given by

$$\begin{aligned}\gamma_{xz}(a,b) = &-\frac{2}{9}C\left(J_{11}^{-1}\right)^2 b(b+1)(b-1)\left(5-27a^2\right)+\\ &-\frac{2}{9}CJ_{11}^{-1}J_{12}^{-1}(b+1)(b-1)a\left(9a^2-5\right)\end{aligned} \tag{160}$$

$$\begin{aligned}\gamma_{yz}(a,b) = &-\frac{2}{9}C\left(J_{21}^{-1}\right)^2 b(b+1)(b-1)\left(5-27a^2\right)+\\ &-\frac{2}{9}CJ_{21}^{-1}J_{22}^{-1}(b+1)(b-1)a\left(9a^2-5\right)\end{aligned} \tag{161}$$

Similarly, for Kirchhoff fields up to third order in the transverse natural coordinate, *a*, i.e. for *p* less than or equal to three, and of fourth order in the longitudinal natural coordinate, *b* , i.e. for *q* equal to four, we obtain spurious shear strains given by

$$\gamma_{xz}(a,b) = -4CJ_{12}^{-1}a^p b(b+1)(b-1) \tag{162}$$

$$\gamma_{yz}(a,b) = -4CJ_{22}^{-1}a^p b(b+1)(b-1) \tag{163}$$

Finally, if we evaluate the spurious shear strain produced by the isoparametric spline finite strip method, subjected to a Kirchhoff field of fourth order in both the natural coordinates *a* and *b*, i.e. for *p* and *q* equal to four, we obtain

$$\gamma_{xz}(a,b) = -\frac{2}{9}C\left(J_{11}^{-1}\right)^2 b(b+1)(b-1)\left(5-27a^2\right) + \\ -\frac{10}{9}CJ_{11}^{-1}J_{12}^{-1}(b+1)(b-1)a\left(9a^2-5\right) + \\ -\frac{4}{9}C\left(J_{12}^{-1}\right)^2 b(b+1)(b-1)\left(10a^2-1\right) \tag{164}$$

$$\gamma_{yz}(a,b) = -\frac{2}{9}C\left(J_{21}^{-1}\right)^2 b(b+1)(b-1)\left(5-27a^2\right) + \\ -\frac{10}{9}CJ_{21}^{-1}J_{22}^{-1}(b+1)(b-1)a\left(9a^2-5\right) + \\ -\frac{4}{9}C\left(J_{22}^{-1}\right)^2 b(b+1)(b-1)\left(10a^2-1\right) \tag{165}$$

As for the case of Hermite sampling scheme, the spurious shear strains expressions given by (160)-(165) equal zero when evaluated at the nodes of the grid given by the following lines

$$a+\frac{\sqrt{5}}{3}=0 \tag{166}$$
$$a=0 \tag{167}$$
$$a-\frac{\sqrt{5}}{3}=0 \tag{168}$$
$$b+1=0 \tag{169}$$
$$b=0 \tag{170}$$
$$b-1=0 \tag{171}$$

This suggest that if reduced integration is performed at the nodes of the grid given by (166)-(171), and shown in Fig. 12, the isoparametric spline finite strip is able to perform without developing spurious shear strain for fourth order Kirchhoff fields given by (113).

The case of a thin plate in uni-axial pure bending is studied. The thin plate has a side length equal to 2*l*, is simply supported at the transverse edges, $y = -l$ and $y = l$, free along the longitudinal edges, and loaded by uniformly distributed bending moments, m_y, acting on the supported edges (Fig. 13).

The material is assumed isotropic and characterised by a Poisson ratio equal to zero. Under these assumptions, the applied moments introduce a uniform bending moment distribution, m_y, within the plate and, consequently, a deformed shape characterised by a constant longitudinal curvature, χ_y, i.e. by a deflection *w*

$$w = \tilde{C}y^2 \tag{172}$$

where $\tilde{c}$ is a constant.

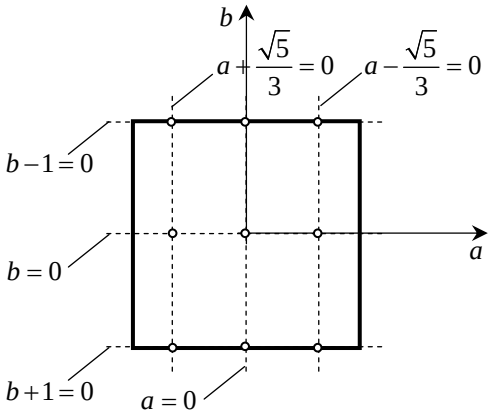

Fig. 12: Modified reduced integration points for the sampling scheme adopted in the computer program.

The plate is firstly modelled by four rectangular isoparametric spline finite strips, Fig. 14 (0), and analysed to provide a reference solution because in case of non-deformed strips no spurious shear strains develop. The isoparametric spline finite strip mesh is then distorted to various degrees: linear distortion, Fig. 14 (1); quadratic distortion, Fig. 14 (2); and cubic distortion, Fig. 14 (3). Three different integration techniques are compared: full integration, reduced Gaussian integration, and a reduced integration technique, modified according to (166)-(171) and Fig. 12.

Fig. 15 shows the numerical results for the deflection at the centre, normalised with respect to the exact solution, for different degrees of distortion. As expected, for regular rectangular strips (level of distortion equal to zero), no locking occurs regardless of the integration scheme adopted and the numerical solution coincides with the exact solution (normalised deflection equal to one). In regular strips, the relation between global coordinates, *x* and *y*, and natural coordinates, *a* and *b*, is given by

$$x = c_{x0} + c_{x1} a \tag{173}$$

$$y = c_{y0} + c_{y1} b \tag{174}$$

Consequently, the Kirchhoff field in natural coordinates, *a* and *b*, for the analysed problem (172), is given by

$$w = C_0 + C_2 b + C_5 b^2 \tag{175}$$

which is included in the set of Kirchhoff fields given in (98).

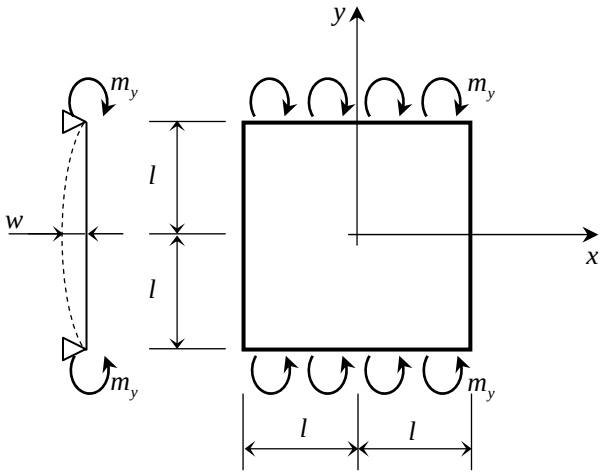

Fig. 13: Shear locking test.

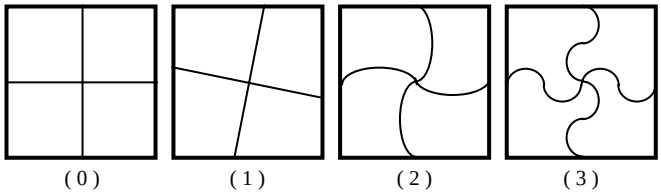

Fig. 14: Different level of distortion analysed.

Shear locking is also not developed, regardless of the integration scheme, for linear distortion. The relation between global coordinates, x and y, and natural coordinates, a and b, is given by

$$x = c_{x0} + c_{x1}a + c_{x2}b + c_{x3}ab \tag{176}$$

$$y = c_{y0} + c_{y1}a + c_{y2}b + c_{y3}ab \tag{177}$$

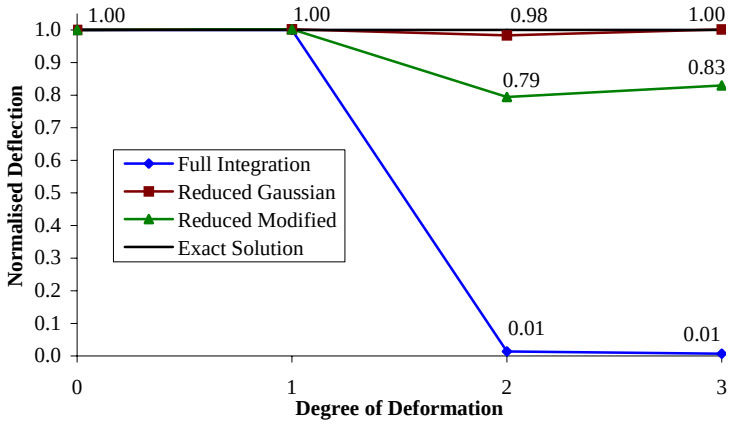

Fig. 15: Performance of the ISFSM with regard to strip distortion.

Consequently, the Kirchhoff field in natural coordinates, a and b, for the analysed problem, see (172), is given by

$$w = C_0 + C_1a + C_2b + C_3ab + C_4a^2 + C_5b^2 + C_6a^2b + C_7ab^2 + C_8a^2b^2 \tag{178}$$

which is included in the Kirchhoff fields given in (98).

When the degree of distortion is quadratic, the geometric mapping is given by

$$x = c_{x0} + c_{x1}a + c_{x2}b^2 + c_{x3}ab^2 \tag{179}$$

$$y = c_{y0} + c_{y1}b + c_{y2}a^2 + c_{y3}a^2b \tag{180}$$

and the corresponding Kirchhoff field in natural coordinates becomes

$$\begin{aligned} w = {} & C_0 + C_2 b + C_4 a^2 + C_5 b^2 + C_6 a^2 b + C_8 a^2 b^2 + \\ & + C_{16} a^4 + C_{18} a^4 b + C_{20} a^4 b^2 \end{aligned} \tag{181}$$

The last three coefficients of (181) belong to the set of Kirchhoff fields given in (113) and it has been proved that for those fields, spurious shear strains develop, except at the reduced points given in (166)-(171). The strip locks when full integration is performed, providing only one percent of the exact solution. Reduced integration performed at the Gaussian points yields accurate results (approximately two percent error), implying that the amplitude of the spurious shear strains at the reduced Gaussian points is small and leading to little stiffening effects in the energy formulation. A much larger error, approximately 21 percent, is introduced if the modified reduced integration, given in Fig. 12, is performed even though spurious shear strains do not develop in this case.

Finally, cubic distortion introduces higher order terms which compromise even further the performance if full integration is performed, while both types of reduced integration perform better than in the case of quadratic distortion.

Spurious shear strains in strips with multiple longitudinal sections

It is of practical interest to evaluate the performance of the element when the number of sections, *m*, varies. Unfortunately, by varying the number of sections, *m*, the sampling scheme changes and, consequently, also the points where the spurious shear strain is zero. In the following, we report the results obtained for a two sections strip required to model a Kirchhoff field of fourth order in both the transverse natural coordinate, *a*, and in the longitudinal natural coordinate, *b*. We obtain

$$\gamma_{xz}(a,b) = -\frac{2}{9}C\left(J_{11}^{-1}\right)^2 b(b+1)(b-1)\left(5-27a^2\right) +$$
$$-\frac{2}{9}CJ_{11}^{-1}J_{12}^{-1}(b+1)(3b-1)(4b-1)a\left(9a^2-5\right) + \qquad ,-1\le b\le 0 \quad (182)$$
$$-\frac{2}{9}C\left(J_{12}^{-1}\right)^2 b(b+1)(2b+1)\left(10a^2-1\right)$$

$$\gamma_{xz}(a,b) = -\frac{2}{9}C\left(J_{11}^{-1}\right)^2 b(b+1)(b-1)\left(5-27a^2\right) +$$
$$-\frac{2}{9}CJ_{11}^{-1}J_{12}^{-1}(b-1)(3b-1)(4b+1)a\left(9a^2-5\right) + \qquad ,0<b\le 1 \quad (183)$$
$$-\frac{2}{9}C\left(J_{12}^{-1}\right)^2 b(b-1)(2b-1)\left(10a^2-1\right)$$

$$\gamma_{yz}(a,b) = -\frac{2}{9}C\left(J_{21}^{-1}\right)^2 b(b+1)(b-1)\left(5-27a^2\right) +$$
$$-\frac{2}{9}CJ_{21}^{-1}J_{22}^{-1}(b+1)(3b-1)(4b-1)a\left(9a^2-5\right) + \qquad ,-1\le b\le 0 \quad (184)$$
$$-\frac{2}{9}C\left(J_{22}^{-1}\right)^2 b(b+1)(2b+1)\left(10a^2-1\right)$$

$$\gamma_{yz}(a,b) = -\frac{2}{9}C\left(J_{21}^{-1}\right)^2 b(b+1)(b-1)\left(5-27a^2\right) +$$
$$-\frac{2}{9}CJ_{21}^{-1}J_{22}^{-1}(b-1)(3b-1)(4b+1)a\left(9a^2-5\right) + \qquad ,0<b\le 1 \quad (185)$$
$$-\frac{2}{9}C\left(J_{22}^{-1}\right)^2 b(b-1)(2b-1)\left(10a^2-1\right)$$

Similar results are obtained in modelling a Kirchhoff field of fourth order in the transverse natural coordinate, *a*, and of an order less than or equal to three in the longitudinal natural coordinate, *b*. From the calculations, the corresponding shear strains are given by

$$\gamma_{xz}(a,b) = -\frac{2}{9}C\left(J_{11}^{-1}\right)^2 b(b+1)(b-1)\left(5-27a^2\right) \qquad ,-1\le b\le 0 \quad (186)$$

$$\gamma_{xz}(a,b) = -\frac{2}{9}C\left(J_{11}^{-1}\right)^2 b(b+1)(b-1)\left(5-27a^2\right) \qquad ,0<b\le 1 \quad (187)$$

$$\gamma_{yz}(a,b) = -\frac{2}{9}C\left(J_{21}^{-1}\right)^2 b(b+1)(b-1)\left(5-27a^2\right) \qquad ,-1\le b\le 0 \quad (188)$$

$$\gamma_{yz}(a,b) = -\frac{2}{9}C\left(J_{21}^{-1}\right)^2 b(b+1)(b-1)\left(5-27a^2\right) \qquad ,0<b\le 1 \quad (189)$$

Finally, if a Kirchhoff field up to third order in *a* and of fourth order in *b* is modelled, the corresponding shear strains are given by

$$\gamma_{xz}(a,b) = -\frac{2}{9} C \left(J_{12}^{-1} \right)^2 b(b+1)(2b+1)\left(10a^2 - 1\right) \qquad , -1 \le b \le 0 \qquad (190)$$

$$\gamma_{xz}(a,b) = -\frac{2}{9} C \left(J_{12}^{-1} \right)^2 b(b-1)(2b-1)\left(10a^2 - 1\right) \qquad , 0 < b \le 1 \qquad (191)$$

$$\gamma_{yz}(a,b) = -\frac{2}{9} C \left(J_{22}^{-1} \right)^2 b(b+1)(2b+1)\left(10a^2 - 1\right) \qquad , -1 \le b \le 0 \qquad (192)$$

$$\gamma_{yz}(a,b) = -\frac{2}{9} C \left(J_{22}^{-1} \right)^2 b(b-1)(2b-1)\left(10a^2 - 1\right) \qquad , 0 < b \le 1 \qquad (193)$$

The numerical integration of the isoparametric spline finite strip is performed independently within each section, i.e. first in the natural longitudinal domain [-1,0] and then in the longitudinal natural domain [0,1] as shown in Fig. 16.

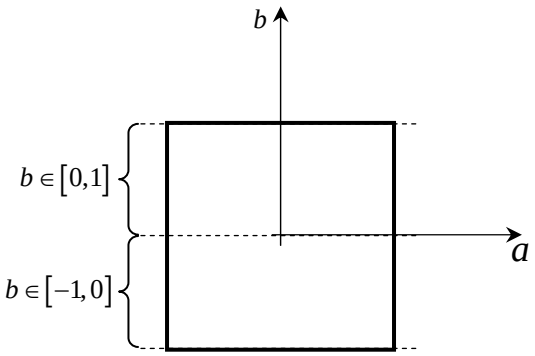

Fig. 16: Isoparametric spline finite strip integration domains for m = 2.

It proves impossible to define a set of reduced integration points, within each integration domain, where all terms in the spurious shear strain expressions given in (182)-(185) are zero. A possible modified reduced integration scheme, consistent with the case of *m* = 1, would be the one given by the nodes of the grid given by the vertical lines

$$a + \frac{\sqrt{5}}{3} = 0 \qquad (194)$$

$$a = 0 \qquad (195)$$

$$a - \frac{\sqrt{5}}{3} = 0 \qquad (196)$$

and by the horizontal lines

$$b+1=0 \tag{197}$$

$$b+\frac{1}{2}=0 \tag{198}$$

$$b=0 \tag{199}$$

for the longitudinal natural domain [-1,0], and by the horizontal lines

$$b=0 \tag{200}$$

$$b-\frac{1}{2}=0 \tag{201}$$

$$b-1=0 \tag{202}$$

for the longitudinal natural domain [0,1], as shown in Fig. 17.

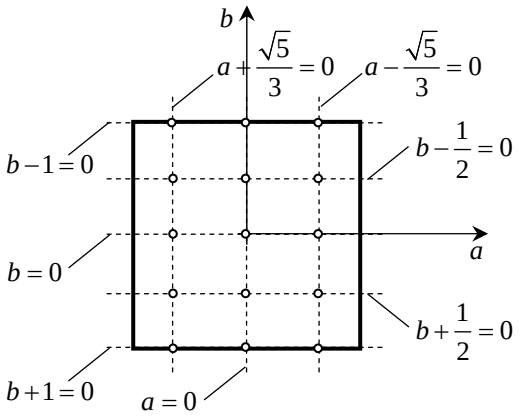

Fig. 17: Modified reduced integration points for m = 2.

The integration scheme will eliminate many of the spurious shear strain contributions of (182)-(185) but several non-zero terms remain, introducing stiffening effects. Similar results are obtained for a larger number of sections. Fig. 18 illustrates the stiffening effects as a function of the number of sections, *m*, for the plate bending problem shown Fig. 13. The results are those for quadratic distorted strips obtained using standard Gaussian reduced integration and using modified reduced integration at the interpolation points shown in Fig. 17.

As previously described, for *m* equal to one, modified reduced integration produces over-stiff results because of the loss of accuracy in the integration scheme. For *m* equal to two and *m* equal to three, a significant drop in the accuracy of the isoparametric spline finite strip results can be observed due to the spurious shear strain contributions. For larger numbers of sections, the accuracy of the analysis increases reaching approximately 84% of the exact value for a number of sections equal to 50. It appears from the graph that the accuracy is improved compared with Gaussian reduced integration for $m > 1$. However, evidently, modified reduced integration does not completely solve the

locking problem, and asymptotically, produces the same results as Gaussian reduced integration. Due to its optimal integration qualities for more regularly shaped strips and because Gaussian reduced integration produces nearly exact results for $m = 1$, Gaussian reduced integration is deemed preferable to modified reduced integration. The tests performed in the following sections are therefore based on the Gaussian reduced integration technique.

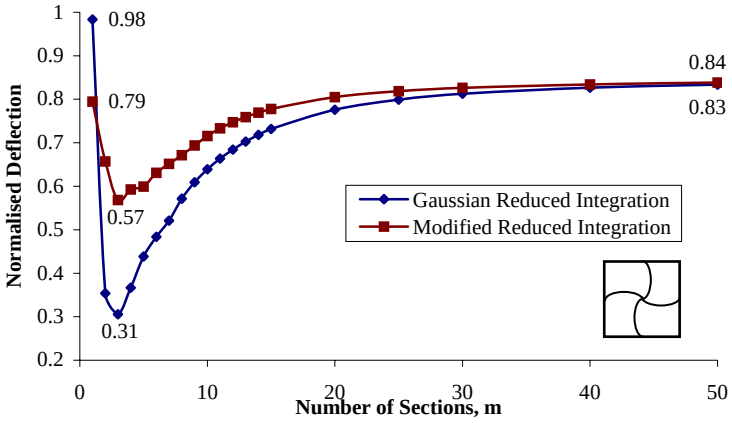

Fig. 18: Stiffening effects due to the longitudinal discretization, quadratic distortion.

Influence of distortion magnitude

It is clear from (182) - (185) that spurious shear strains are directly influenced by the magnitude of the distortion, represented by the components of the inverse of the Jacobian matrix components, J_{11}^{-1}, J_{22}^{-1}, J_{12}^{-1} and J_{21}^{-1}. To investigate the importance of the distortion magnitude, the problem given in Fig. 13 in conjunction with the quadratic distortion shown in Fig. 14 (2) is solved using the Gaussian reduced integration technique for three levels of distortion magnitude. To quantify the distortion of the strip, the ratio between the maximum offset, *d*, between the deformed edge and its linearized projection, and the length of the linear projection itself, *l*, is adopted, as shown in Fig. 19.

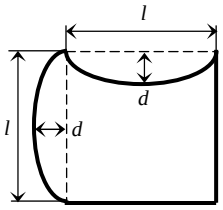

Fig. 19: Measurement of distortion.

Three distortion magnitudes have been considered: a moderate deformation with a deformation ratio, *d/l*, equal to 0.1, a large deformation ratio, *d/l*, of 0.45 and an intermediate case with a deformation ratio, *d/l*, of 0.22. The results in terms of normalised deflection at the centre of the plate are shown in Fig. 20 for a varying number of sections, *m*.

The distortion magnitude affects the performance for any number of sections, *m*. For high distortion magnitudes, the performance is poor regardless the number of sections, *m*, but for a moderate distortion magnitude (*d*/*l* = 0.1), the performance can be considered satisfactory when the number of sections, *m*, exceeds approximately 15.

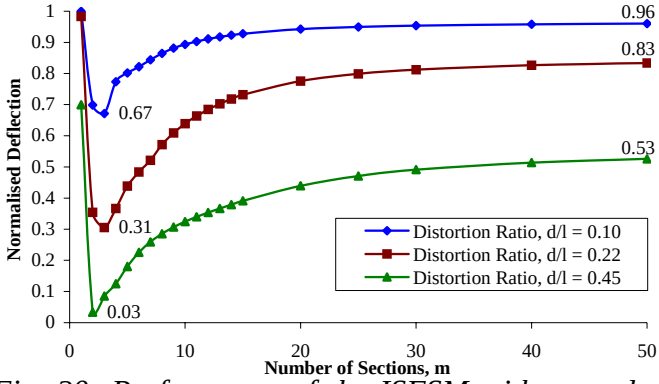

Fig. 20: Performance of the ISFSM with regard to deformation magnitude.

Different cases of quadratic distortions

In practical applications, distorted strip geometries like the ones shown in Fig. 14 (2), Fig. 14 (3) and in Fig. 21 (c) are not very common, while in modelling perforated areas the geometries shown in Fig. 21 (a) and Fig. 21 (b) are often utilised.

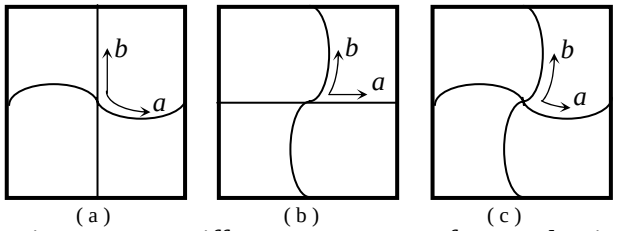

Fig. 21: Different types of quadratic distortions: (a) *distortion along the natural transverse coordinate, a;* (b) *distortion along the natural longitudinal coordinate, b;* (c) *distortion along both natural coordinates, a and b.*

The performance of the isoparametric spline finite strip, if distorted according to the deformations shown in Fig. 21, is tested by analysing a square thin plate, point-supported at the corners and subjected to uniformly distributed bending moments along the four sides (Fig. 22).

The exact deflection Kirchhoff field for the problem given in Fig. 22 is

$$w = \tilde{C}_x x^2 + \tilde{C}_y y^2 \qquad (203)$$

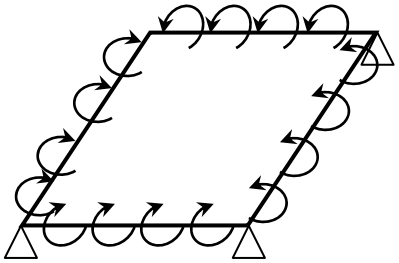

Fig. 22: Test for different types of quadratic deformation when Gaussian reduced integration is performed.

The geometric relations between global coordinates, *x* and *y*, and natural coordinates, *a* and *b*, for the strips in Fig. 21 (a) are

$$x = c_{x0} + c_{x1}a \tag{204}$$

$$y = c_{y0} + c_{y1}b + c_{y2}a^2 + c_{y3}a^2b \tag{205}$$

By substituting (204) and (205) into (203) we obtain the Kirchhoff field in natural coordinates, *a* and *b*:

$$\begin{aligned} w = {} & C_0 + C_1a + C_2b + C_4a^2 + C_5b^2 + C_6a^2b + C_8a^2b^2 + \\ & + C_{16}a^4 + C_{18}a^4b + C_{20}a^4b^2 \end{aligned} \tag{206}$$

Considering now the strip distortion represented in Fig. 21 (b) we obtain the following relations between global and natural coordinates:

$$x = c_{x0} + c_{x1}a + c_{x2}b^2 + c_{x3}ab^2 \tag{207}$$

$$y = c_{y0} + c_{y1}b \tag{208}$$

By substituting (207) and (208) into (203) we obtain the Kirchhoff field in natural coordinates, *a* and *b*:

$$\begin{aligned} w = {} & C_0 + C_1a + C_2b + C_4a^2 + C_5b^2 + C_7ab^2 + C_8a^2b^2 + \\ & + C_{17}b^4 + C_{19}ab^4 + C_{21}a^2b^4 \end{aligned} \tag{209}$$

Finally, for the combined distortion shown in Fig. 21 (c), the geometric relations between global coordinates and natural coordinates are

$$x = c_{x0} + c_{x1}a + c_{x2}b^2 + c_{x3}ab^2 \tag{210}$$

$$y = c_{y0} + c_{y1}b + c_{y2}a^2 + c_{y3}a^2b \tag{211}$$

By substituting (210) and (211) into (203) we obtain the Kirchhoff field in natural coordinates, *a* and *b*:

$$w = C_0 + C_1 a + C_2 b + C_4 a^2 + C_5 b^2 + C_6 a^2 b + C_7 a b^2 + C_8 a^2 b^2 + \\ + C_{16} a^4 + C_{17} b^4 + C_{18} a^4 b + C_{19} a b^4 + C_{20} a^4 b^2 + C_{21} a^2 b^4 \qquad (212)$$

It should be noticed that the last three terms of (206) and (209) and the last six terms of (212) belong to the set of Kirchhoff fields given in (113) which is premised on modified reduced integration. Consequently, when applying Gaussian reduced integration, spurious shear strain contributions are expected to produce shear locking in all distorted strips shown in Fig. 21.

Fig. 23 illustrates the performance of the isoparametric spline finite strip with varying number of sections, *m*. The reference distortion ratio, d/l, is equal to 0.22. In this specific case, it can be observed that the poorest performance is obtained when the strip is distorted in both directions, as shown in Fig. 21 (c). When the distortion is along the transverse natural coordinate, *a*, only, Fig. 21 (a) we observe that the accuracy varies between a maximum of the 100% for a single section and a minimum of 78% for two sections. Asymptotically, the accuracy reaches 93% of the exact value, demonstrating that the shear locking cannot be completely eliminated by longitudinal refinement of the mesh.

A different behaviour is observed for strips distorted along the coordinate *b*, (Fig. 21 (b)). A softening effect of about the 23% is noticed if only one section is employed, while the solution is over-stiff when using two or three sections. By increasing the number of sections, *m*, thus refining the longitudinal mesh, the accuracy is greatly improved for *m* larger than three, reaching the exact solution for *m* approximately equal to 15. The increased accuracy is achieved because, with the longitudinal refinement, the local distortion magnitude reduces significantly within each section.

Finally, to investigate the influence of the distortion magnitude, the test is repeated for the distortion magnitude ratio, d/l, varying from zero to 0.45, for each of the three possible quadratic distortions shown in Fig. 24.

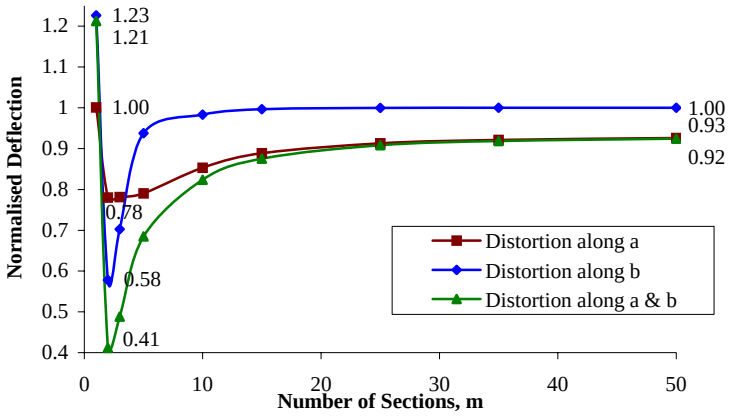

Fig. 23: Performance of the ISFSM for different quadratic distortions of the strip with respect to the number of sections, m.

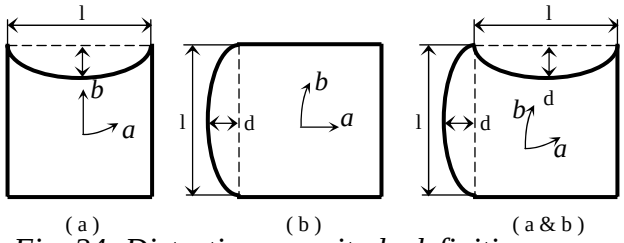

Fig. 24: Distortion magnitude definition.

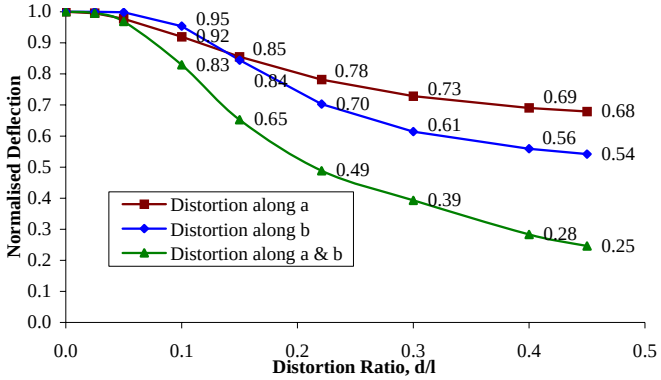

Fig. 25: Performance of the ISFSM for different quadratic distortions of the strip when the distortion magnitude varies.

The results are shown in Fig. 25. It can be observed that overall the sensitivity of the isoparametric spline finite strip to distortions along the transverse natural coordinate, *a*, is not as strong as to distortions along the longitudinal natural coordinate, *b*. The method performs better in the range of moderate distortion magnitudes, if the distortion is along the natural coordinate, *b*, but the accuracy decreases rapidly when the distortion ratio exceeds 0.1. A doubly distorted strip offers the poorest performance also in this case, combining the sensitivity to both distortions.

Conclusions

The tendency of C^0 plate strips to develop shear locking in thin applications has been analysed. It has been stated that shear locking entirely depends on the development of spurious shear strain in the pure flexural displacement fields. An analytical definition of the spurious shear strain has been given along with a test, the monomial test, which allows the performance of an element with regard to its flexural behaviour to be evaluated.

The shear locking performance of the isoparametric spline finite strip method has been investigated. The monomial test has been applied to show that isoparametric spline finite strips do not lock for Kirchhoff fields up to the third order in both the transverse and the longitudinal natural coordinates, *a* and *b*, respectively. For Kirchhoff fields of higher order, spurious shear strains develop. In particular, the performance of Kirchhoff fields of fourth order has been investigated. It has been shown that for these fields, spurious shear strains

are represented by cubic functions in both the natural coordinates, *a* and *b*. The shear strains are zero at specific reduced integration points which depend on the interpolation scheme adopted and on the number of longitudinal sections, *m*, characterising the strip.

Expressions for the spurious shear strains have been derived for a fourth order Kirchhoff field. The expressions are given for three different interpolation schemes, referring to a strip with single longitudinal section, $m=1$. Furthermore, the expressions for the spurious shear strains for a strip with two longitudinal sections, $m=2$.

The influence of spurious shear strains on the accuracy of the isoparametric spline finite strip has been investigated by means of numerical examples. The examples highlight the influence of the numerical integration scheme, the effect of the number of sections, *m*, and the effect of the degree of distortion of the strip.

Gaussian reduced integration proved the most appealing, because of its optimal integration qualities for regularly shaped strips and because it produces nearly exact solutions for a single section, $m = 1$. Modified reduced integration improves the accuracy for $m = 2$ and $m = 3$ but, overall, is not superior to Gaussian reduced integration.

In the case of quadratic (or cubic) distortion, the best performance is obtained when the strip is subdivided into a single longitudinal section. Very good results can also be obtained by refining the longitudinal mesh, i.e. by increasing *m*, in the case of distortions along the longitudinal edges of the strip. For distortion along the transverse edges, a fine finite strip mesh is recommended.

These results provide guidance on the choice of mesh to utilise in the numerical model and, if adhered to, ensure a good performance of the isoparametric spline finite strip in the analysis of complex perforated, or distorted, elements.

References

Briassoulis, D., (1988), *Monomial test: testing the flexural behaviour of degenerated shell element*, Computers and Structures, 29, 6, 949-958

Briassoulis, D., (1989), *On the basics of the shear locking problem of C^0 isoparametric plate elements*, Computers and Structures, 33, 1, 169-185

Eccher, G., Rasmussen, K.J.R., Baldassino, N. and Zandonini, R., (2005), *Isoparametric Spline Finite Strip Method for In-plane Stress Analysis*, The University of Sydney, Department of Civil Engineering.